Electronic Thesis and Dissertation Repository

9-23-2016 12:00 AM

Agglomerate Formation and Heat Transfer study in a Novel Mechanically Fluidized Reactor

Dhiraj M. Kankariya, *The University of Western Ontario*

Supervisor: Dr. Cedric Briens, *The University of Western Ontario*
Joint Supervisor: Dr. Dominic Pjontek, *The University of Western Ontario*
A thesis submitted in partial fulfillment of the requirements for the Master of Engineering Science degree in Chemical and Biochemical Engineering
© Dhiraj M. Kankariya 2016

Recommended Citation

Abstract

The aim of the thesis was to study two important features of the Mechanically Fluidized Reactor (MFR): the good distribution of injected liquid on fluidized particles and the high heat transfer rate from the heated wall to the bed. Multiple industrial processes use liquid injection in fluidized bed reactors. The liquid distribution in the reactor should be efficient to minimize bed defluidization and to maximize the yield and quality of the products.

The study used two MFR units, with internal volumes of 1.0 and 4.42 litre, respectively. Induction heating was used to rapidly heat the bed, which is a unique feature of the system.

To characterize the distribution of injected liquid, an experimental method measured the amount of liquid trapped in agglomerates and the mass of agglomerates. The amount of liquid trapped in agglomerates decreased with increasing impeller rotation speed. The best impeller speed to achieve nearly perfect liquid distribution, with only 1 wt.% of the injected liquid trapped in agglomerates, was 130 rpm.

To study wall to bed heat transfer, temperature measurements for the small MFR were used to estimate the overall heat transfer coefficients. It was observed that the overall heat transfer coefficient increased significantly with increasing particle size and a strong influence of the superficial velocity of the vaporized liquid on the heat transfer coefficients was noted. The wall to bed heat transfer coefficient was typical of the values that can be achieved with traditional bubbling fluidized beds, even at vapour velocities below the minimum fluidization velocity.

Keywords

Co-authorship statement

Chapter 5

Article title:
Effect of reactor volume, particle size and material on heat transfer in a mechanically fluidized reactor
Authors:
Dhiraj M. Kankariya, Stefano Tacchino, Cedric Briens, Dominic Pjontek
Article status:
Unpublished
Contributions:
Dhiraj M. Kankariya, Stefano Tacchino performed all experimental work and design. Data analysis is done by Dhiraj M. Kankariya. Review of this work is given by Cedric Briens and Dominic Pjontek.

Acknowledgement

I am very thankful to my supervisors Dr. Cedric Briens, Dr. Dominic Pjontek for the opportunity to work with them. Their support, guidance and friendly mentorship at all the times was of great help.

I would like to specially thank to and appreciate for all the help by Dr. Francisco J. Sanchez Careaga, Dr. Stefano Tacchino, Tom Johnston and my colleagues at ICFAR.

Mom, Dad this is especially because of and for you.

Thanks to my family and friends!

Table of Contents

List of Tables

List of Figures

List of Symbols

$A_L = Area\ of\ heat\ losses\ (m^2)$

$Avg.\,T_{bed} = Average\ of\ the\ particle\ bed\ temperature\ in\ the\ reactor\ (°C)$

$c = Specific\ heat\ capacity\ of\ fluidized\ solids\,(\dfrac{KJ}{kg.\,K})$

$c_g = Specific\ heat\ capacity\ of\ gas\ (\dfrac{KJ}{kg.\,K})$

$C_{P_L} = Specific\ heat\ of\ water\ (\dfrac{kJ}{kg.\,K})$

$Cp_v = Specific\ heat\ of\ steam\ (\dfrac{kJ}{kg.\,K})$

$d_{aggl} = Agglomerate\ diameter\ (\mu m)$

$d_p = Particle\ diameter\ (\mu m)$

$d_{p_{sm}} = Sauter\ Mean\ Diameter\ (\mu m)$

$F_L = Flow\ rate\ of\ the\ liquid\ (\dfrac{ml}{min})$

$g = Acceleration\ due\ to\ gravity\ (\dfrac{m}{s^2})$

$I = Electric\ current\ (A)$

$k_g = Gas\ thermal\ conductivity\ (\dfrac{W}{m.\,K})$

$k_m = Thermal\ capacity\ of\ quiescent\ bed\ (\dfrac{W}{m.\,K})$

l_t = Turbulent flow length scale (m)

$\dfrac{L}{S}$ = Liquid to Solid ratio

m_{sand} = Mass of the washed and dried sand particles (g)

MFR = Mechanically Fluidized Reactor

R = Resistance of the heater acrtridge (Ω)

S = Stirring factor accounting for type of bed motion

T_1 = Temperature of the wall in the top part of the reactor (℃)

T_2 = Temperature of the wall in the center part of the reactor (℃)

T_3 = Temperature of the wall in the bottom part of the reactor (℃)

T_4 = Temperature of the vapor exiting from the vapor exit hole in the reactor (℃)

T_5 = Temperature of the vapor in the freeboard region of the reactor (℃)

T_{bed} = Particle bed temperature in the reactor (℃)

T_{room} = Room temperature (℃)

T_{SP} = Temperature set point of the bed (℃)

T_{wall} = Wall temperature (℃)

$T_{w_{average}}$ = Average wall temperature (measured at 3 location) (℃)

$T_{w_{STDEV}}$ = Standard deviation of wall temperature (measured at 3 location) (℃)

U = Overall heat transfer coefficient ($\dfrac{W}{m^2.K}$)

$U_{average}$ = Average of overall heat transfer coefficient values measured at

different rpm for mixing at a selected liquid flowrate ($\frac{W}{m^2.K}$)

$U_{correlation}$ = Oveall heat transfer coefficient from the Molerus correlation ($\frac{W}{m^2.K}$)

U_{max} = Maximum of all overall heat transfer coefficient values measured at

different rpm for mixing at a selected liquid flowrate ($\frac{W}{m^2.K}$)

U_L = Overall heat transfer losses ($\frac{W}{m^2.K}$)

x = Absorbance of the agglomerates for a particular size cut

x_f = Weight fraction of the fines (g)

x_{fbed} = Weight fraction of the fines in the initial silica sand (g)

λ_{max} = Characteristic wavelength of a dye colour

$\sigma_{T_{bed}}$ = Standard deviation of the particle bed temperature in the reactor ($°C$)

δ_d = Time fraction heat transfer surface is occupied by particle packets

ρ_g = Gas density ($\frac{kg}{m^3}$)

ρ_m = Density of quiescent solids ($\frac{kg}{m^3}$)

ρ_p = Particle density ($\frac{kg}{m^3}$)

$\Delta H_{v_{ref}}$ = Latent heat of vaporisation (reference)($\frac{kJ}{kg}$)

$$Ar = Archimedes\ number = d_p{}^3(\rho_p - \rho_g)\rho_g g/\mu^2$$

List of Appendices

CHAPTER 1

1 INTRODUCTION

Agglomerate formation has been extensively studied for many industrial processes, in the food, oil and gas, pharmaceutical and fertilizers sectors, which employ wet agglomeration in a gas-solid fluidized bed. It is important to have a proper liquid distribution, along with other conditions, in the reactor to enlarge or minimize the agglomerate size, depending on the process, to obtain a final product with desired characteristics, quality and yield. Several studies (Reyes, 2015) focusing on binder characteristics and operating conditions have been performed to better understand the liquid distribution on the solids.

Agglomeration should be minimized in the thermal cracking reactors used for biomass conversion (torrefaction, pyrolysis, gasification) and heavy oil coking (Bridgwater, 2012). Due to the good gas-solid mixing and heat and mass transfer properties of the fluidized bed reactors, they are the most suitable and widely used industrial reactors for thermal cracking (McKendry, 2002). This work focuses on agglomerate formation and heat transfer characteristics to better understand fluidized thermal cracking reactors (e.g., Fluid Cokers, pyrolysis reactors).

1.1 Fluidized thermal cracking reactors

Fluid Coking^{TM} is an industrial process where the liquid feed is injected into gas-solid fluidized bed reactors. The important components of the Fluid Coking^{TM} process are: the reactor, stripping section, scrubbing section and the burner. In the Fluid Cokers, heavy bituminous hydrocarbons are atomized with steam into a hot fluidized bed of coke, which provides the heat required to convert liquid feed into cracked hydrocarbon vapors (McCaffrey et al., 1998). The liquid does not vaporize rapidly in Fluid Cokers, as the reaction temperature is lower than the boiling temperature of the heavy bituminous feed. For vaporization to occur, liquid has to be thermally cracked into smaller fragments by contacting of a heat carrier, which in this case are the solid particles.

A stripper section is used to minimize the hydrocarbons being carried into the burner vessel by stripping them from the bed coke surface. Gray (2002) studied that the coke grows in size due to the formation of fresh layers, coupled with agglomeration of wetted particles. Due to poor liquid distribution agglomerates are formed and they will segregate in the bottom section, pass through the stripper section and will carry unreacted liquid inside the burner, thereby, reducing the overall yield. The burner partially combusts the coke with oxygen to generate the heat required for sustaining the endothermic cracking reactions and the coke is then recycled into the reactor. Excess coke is then quenched and stockpiled to be used in the future (Hammond et al., 2003). The scrubber condenses the product oil, which is then processed downstream (Soskind et al., 1982). Coke, condensable product oil and non-condensable gases are the final products obtained from the Fluid Cokers.

House et al. (2004, 2008) showed that the formation of coke-bitumen agglomerates can have a considerable impact on the cracking reactions in Fluid Cokers. An excellent characteristic of fluidized beds is their solids mixing ability. Fluid Coking^{TM} in itself is not intended as a wet-agglomeration process, but it can be considered so due to the injection of bitumen in the process, which acts as a liquid binder of the coke particle aggregates (Gray, 2002). Agglomerate formation results in two main problems in Fluid Cokers: the yield of valuable liquids is reduced (Stanlick, 2014) and large wet agglomerates can reach the stripping section, fouling the stripper sheds and leading to premature shut-down (House et al., 2006).
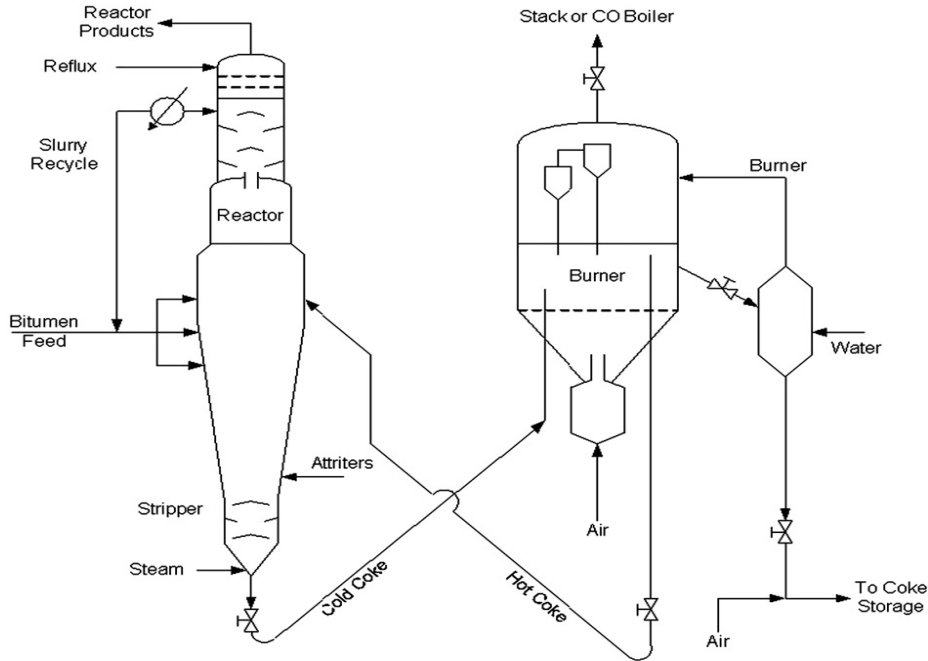
Figure 1-1: Fluid Coker (House et al., 2008).

1.2 Mechanically Fluidized Reactor (MFR)

Lago et al. (2015) studied the mixing characteristics of a Mechanically Fluidized Reactor (MFR) which was developed for fast pyrolysis of biomass. They investigated stirrer geometries including the spiral stirrer, vertical blades stirrer and the paddle stirrer. The stirrer provides the desired mixing between the bed material and the injected biomass in the reactor, while effectively breaking agglomerates. Furthermore, effective mixing between the bed and the heaters is crucial to achieve effective heat transfer between the bed and the injected biomass particles. The vertical blades stirrer was found to be the most suitable stirrer resulting in the smallest power consumption (Lago et al., 2015), while also requiring the lowest torque. The pyrolysis tests performed in the MFR highlighted the improved mixing ability of the vertical blade stirrer as it reduced the time required for pyrolysis at all the rotation speeds. Lago et al. (2015) demonstrated that heat transfer between the hot bed material and the biomass pellets was improved with the vertical blade stirrer. A main feature of the vertical blade stirrer is that it brings reacting particles in the lower region of the reactor bed, so that vapors and gases generated by their reaction help aerate the bed.

Chaudhari (2012) studied liquid-solid contact in the MFR using a new method called dissipation time (t_d). The method is based on the flowrate measurement of the product vapors exiting the MFR, by using an orifice assembly. The liquid-solid contact in the MFR was improved when increasing the agitation rate. Similarly, increasing the MFR temperature improved liquid-solid contact, whereas liquid-solid contact was degraded when augmenting the liquid flowrate. The yield of valuable liquid product increased with improved liquid-solid contact, demonstrating the importance of liquid-solid mixing in the MFR. This improvement in the liquid-solid contact was due to the increased rotational speed of the agitator. As the agitator speed was increased, more particles were exposed to the liquid. With perfect liquid-solid contact, no agglomerates would be formed and the dissipation time would be zero. But if the contact between the liquid-solid worsens, then larger and wetter agglomerates would be formed and, as the wetter agglomerates are stronger, the dissipation time would be increased (Weber et al., 2011).

Another study (Stanlick, 2014) used an MFR to investigate bitumen thermal cracking, while varying the vapor phase residence time to study the impact of vapor thermal cracking on the product quality. It was observed during the study that the mechanical agitation in the MFR significantly reduced the agglomerate sizes in the agglomerating system of bitumen thermal cracking.

Various fluidization regimes (Daizo and Levenspiel, 1991) obtained when the velocity of the gas flowing through a bed of solid particles is increased are:

    i)   *Particulate regime*: In this regime, the bed is fluidized without appearance of the gas bubbles and there is an intimate mixture of gas and particles.

    ii)   *Bubbling regime*: The gas bubbles formed rise and coalesce to form larger bubbles which may then split and recombine. As the gas velocity increases, the bubbles become larger. Also, the bubbles contain almost no particles but they carry particles in their wakes which induces intense solid mixing.

    iii)   *Slugging regime*: In this regime, the bubbles continue growing until they fill most of the column cross-section and there are almost no solids in the slugs. As the wakes are small, they do not carry much solids. Thus, the solid mixing is less intense.

iv) *Turbulent fluidization*: In this transition regime, the gas is flowing as small elongated voids. It constantly appears and disappears. The solid mixing in this regime is rapid.

v) *Fast fluidization*: The solids entrained are recycled to the bottom of the column by a cyclone. There is no bed surface as the solid entrainment is very large and the mixing of solids is rapid.

vi) *Pneumatic transport*: When there is no recycling of the solids then pneumatic transport occurs instead of fast fluidization.

1.3   Agglomeration

Agglomerates are groups of particles which are formed when smaller individual particles are joined by binding them. This new larger particle is one in which the original particles can still be seen (Parveen et al., 2012).

1.3.1   Wet agglomeration

Wet agglomeration is the process in which a liquid binder is used to cluster the particles together. A liquid binder can be sprayed on a group of particles, which are moving or are agitated, to promote their adhesion by viscous forces and solid bridges as the liquid is evaporated (Iveson et al., 2001). Typically, gas-solid fluidized beds are used due to their improved solids mixing and approximately uniform temperature (Woollard and Potter, 1968), thereby, leading to the uniform evaporation of solvent used for binder distribution. There are many reasons to forming agglomerates, such as achieving high quality product appearance, increasing the bulk density for storage, control of characteristics such as solubility (Mehta et al., 2005). In the case of Fluid Coking^{TM}, for example, the presence of agglomerates affects the operability by fouling the internals and reducing the yield. Also, for a pyrolysis reactor, heat transfer is an important parameter as it helps understand how quickly the reactor can transfer heat to the biomass. The gas convective component, particle convective component and radiation are the principal mechanisms of heat transfer between the heat transfer surfaces and the bed (Botterill, 1975). The drying of wet agglomerates in fluidized bed dryers/granulators and the transfer of heat to the wet agglomerates in a fluid coker are the practical examples of heat transfer between a large particle and a fluidized bed.

It is difficult to quantitatively predict the agglomerate or granule attributes (Iveson et al., 2001). Different mechanisms have been used to describe the formation and break-up of agglomerates. Differentiation between these mechanisms largely depends on the cut-off size between agglomerate and non-agglomerate materials. There are generally three sets of rate processes to determine the wet granulation behavior (Iveson et al., 2001), illustrated in **Figure 1-2.**

i) *Wetting & nucleation*: The distribution of liquid over the moving particles, which then forms "seeds" for the subsequent agglomerates (nuclei). Nuclei kinetics depend on solids mixing and liquid properties. Nuclei formation mechanism is highly dependent on the size of the liquid droplet. If the droplet is bigger than the individual sand particle, the nuclei will then form by immersion, whereas for droplet sizes smaller than the individual particle then the nuclei formation takes place by dispersion.

ii) *Consolidation & coalescence*: Particles agglomerate due to collisions between granules and other granules (coalescence) and/or individual particles (layering). Liquid properties have an impact on the consolidation strength. The mechanical properties of the granules also affect the consolidation strength. Agglomerate strength is determined by the capillary forces, inter-particle forces and the viscous forces (Iveson and Page, 2001). In most cases, the capillary forces have more impact than the viscous forces. The temperature of the bed and the droplet velocity affects the consolidation of agglomerates.

iii) *Attrition & breakage*: Breakage and attrition occurs in fluidized beds due to shear forces, and thermal or chemical changes (Ayazi Shamlou et al., 1990). Due to intense mixing, the breakage rate can be high in the reactor vessel (Iveson and Page, 2001). When using a high-shear mixer granulator, the geometry of the mixing blades and the bed temperature can significantly impact agglomerate breakup (Benali et al., 2009).

(i) Wetting & Nucleation

(ii) Consolidation & Coalescence

(iii) Attrition & Breakage
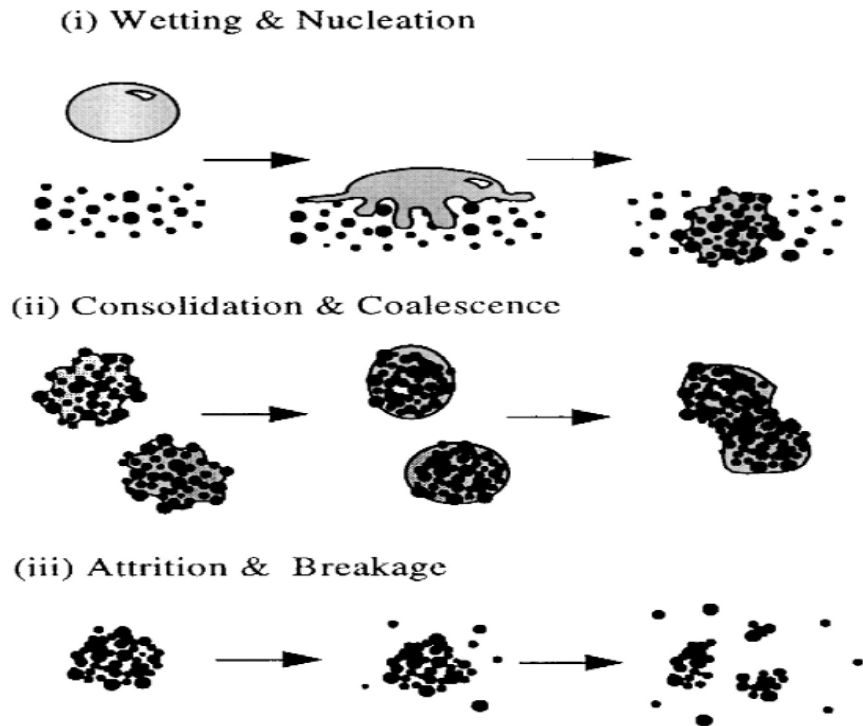
Figure 1-2: Mechanisms of agglomeration process (adapted from Iveson et al. (2001)).

1.3.2 Agglomerate formation and liquid-solid contact in fluidized beds

Weber et al. (2011) showed that at lower temperatures in a fluidized bed, a higher amount of liquid is available for a longer duration as the rate of thermal cracking is reduced. A large fraction of the fed bitumen is reacted and devolatilized, while the remainder can be incorporated in the formation of agglomerates. The growth, erosion and fragmentation of agglomerates in the fluidized bed was studied. Complicated interactions of several parameters affecting the previous phenomena were observed. For example, a transition from negligible agglomerate fragmentation to complete fragmentation, including an intermediate transition region, was achieved by increasing the superficial gas velocity or agitation in the reactor. Weber et al. (2008) also observed that the smaller agglomerates were more easily eroded when compared to the larger agglomerates.

Weber et al. (2011) observed that an increase in the initial agglomerate size greatly influenced agglomerate survival in the fragmentation regime, but has a negligible impact in the no-fragmentation regime. Larger agglomerates were fragmented into smaller clusters, thereby

increasing the quantity of smaller fragments. This demonstrates that larger agglomerates experienced greater erosion, causing them to lose more relative mass than smaller agglomerates. According to Gray (2002), if the film thickness of bitumen exceeds 20 microns, at a reactor temperature of 530℃, then mass transfer limitations will be present. Liquid-solid contact in fluid coking is thus quantified based on the liquid feed fraction forming granules, the agglomerate sizes, and liquid-solid ratio in the granules. Also, when a feed droplet enters the fluidized bed, it impacts multiple particles as it is larger than the bed particles. At the Fluid Coking gas velocities (0.3-1.5 m/s), the resulting granule when liquid engulfs the coke particle becomes unstable and is pulled apart or broken up due to the shear forces prior to exiting the reactor.

A mechanism was proposed by Gray (2002) for the distribution of feed from large droplets to smaller heat-carrier particles, which requires the wet granules to be unstable under fluidization condition. Agglomerate break-up will occur if the internal cohesive forces within the granule are smaller than the external forces exerted on the granule by the collisions with other bed particles. The wet feed in the reactor account for the interparticle forces due to the liquid bridges between the particles. In the case of larger diameter particles, the previous forces dominate over the Van der Waals and electrostatic forces, which are significant for finer particles.

According to McMillan et al. (2013), particle clustering is extensive for the fluidized bed systems and their formation can be due to the collisional cooling, van der Waals forces, coulomb forces, hydrodynamics and cohesive bridging. Collisional cooling only dominates in the absence of other interparticle forces. The result of dipole interaction between two objects is the van der Waals force, which is a short-ranged force and the particles must be close for such forces to take hold. Hydrodynamics are due to the drag force. The drag when particle interacts with the fluid results in shedding of eddie currents or streams that can attract other particles. The heterogeneity in the fluid dynamics, caused by the drag results in particle clustering.

1.3.3   Agglomerate measurement method

Several experimental models have been developed to study the behavior and formation of agglomerates under safe, low temperature, conditions that simulate the high temperature processes in Fluid Cokers.

A previous study investigated the effect of viscosity on agglomerate formation in a shear mixer (Schæfer and Mathiesen, 1996). Mechanisms for the initial wetting of particles by injection of a liquid droplet were proposed. One mechanism explains the wetting by distribution, where liquid droplets are distributed on the surface of particles in the surrounding forming the initial nuclei. It was observed that the mechanism dominates when the droplets and particles are of similar size. Another mechanism explains the wetting by immersion, where the initial nuclei is formed by large droplets engulfing the individual particles.

House et al. (2008) first used a sugar solution to study agglomeration in fluidized beds at room temperature. Simulation of the Fluid Cokers evaporation and agglomeration processes was experimentally studied by using a sugar solution at high bed temperatures to achieve caramelization conditions (Saha, 2012). The solidified agglomerates were recovered for analysis; however, the high temperature (up to 250°C) sugar caramelization reaction made it difficult to properly measure the agglomerate liquid content.

Reyes (2015) developed an experimental model and an associated measurement method to study the formation of agglomerates and their stability in the fluidized beds. Preliminary tests in a small fluidized bed reactor compared the agglomerate properties obtained with the model and actual Fluid Coking of bitumen. Studies were then performed in a larger pilot plant scale reactor to analyze the effects of various parameters, such as bed temperature and binder viscosity, on the total mass, size distribution and internal liquid concentration of agglomerates. It was observed that greater average bed temperature during injection resulted in greater agglomerate formation, with agglomerates were larger and had a higher liquid content. At lower temperatures, liquid evaporation was slower, providing more time for the agglomerates to break up, resulting in drier agglomerates.

1.4   Previous studies on Heat Transfer in a Fluidized Bed reactor

Pyrolysis, Fluid Coking and other thermal cracking reactors usually need to transfer heat from a heat exchange surface, such as the reactor wall, to the reactor bed, since significant heat is required to convert the solid or liquid feedstock to hot, cracked product vapors. Bubbling and

turbulent fluidized beds are a popular solution for these types of process as they provide good wall to bed heat transfer (Daizo and Levenspiel, 1991).

Many correlations are available to estimate the heat transfer coefficients (Syamlal and Gidaspow, 1985), but these correlations have limitations and are generally only applicable for select experimental conditions. In some cases, the correlations may differ from the actual coefficients by up to two orders of magnitude (Gelperin and Ainshtein, 1971). Molerus et al. (1995) proposed a correlation that allows to predict the heat transfer coefficient based on its dependence on the superficial velocity of gas.

The bed material must be selected to ensure good wall-to-bed heat transfer. Surface to bed heat transfer was studied using several fine bed materials such as polymers, quartz sand, ballotini, corundum and carborundum (Di Natale et al., 2009). The tests point out that the heat transfer coefficient increases with particle Archimedes number. The different polymeric powders tested were shown to have an increase in the heat transfer coefficient with an increase in the particle size at the gas velocity of 0.1 m/s.

It is important to select the best particle size. Reduced particle sizes favor heat transfer both from the wall to the bed and within the particles (either reacting biomass particles or wet agglomerates) (Molerus, 1993). However, with fluidized bed reactors, smaller particles result in larger, undesired entrainment of fines. It is, therefore, important to determine which particle size provides a reasonable compromise between entrainment and heat transfer.

Scale up from laboratory to commerical scale is an important consideration. Stefanova et al. (2011) measured the heat transfer coefficients using an identical vertical heater (an electrically heated copper tube), alumina particles and geometrically scaled bubble-cap distributors in fluidized beds of different diameters. The maximum heat transfer coefficient was found to be independent of the column diameter. The maximum heat transfer coefficient reached in the two columns were similar, but the superficial gas velocities at which the maximum heat transfer coefficient was attained were greater in the case of the larger column.

An important feature of the MFR is that bed mixing and turbulence can be adjusted without changing the particle characteristics and vapor flows through the bed, by changing the mixer rotating speed. A better understanding of the heat transfer properties in the MFR is needed, in particular how they depend on particle properties, bed temperature, impeller mixing speed, and reactor diameter.

Several methods have been used to measure the wall-to-bed heat transfer coefficient in conventional fluidized beds.

The gas convection, particle convection and radiation are the basic mechanisms of heat transfer between the bed and the heat transfer surface (Stefanova et al., 2011). The overall heat transfer coefficient is thus written as;

$$h = (1 - \delta_d)h_g + \rho_d h_{pa} + h_{rad} \tag{1}$$

where $(1 - \delta_d)h_g$ is the gas convection component, $\rho_d h_{pa}$ is the particle convection component and h_{rad} is the radiation component, δ_d is the time fraction heat transfer surface is occupied by particle packets.

Mickley and Fairbanks (1955) concluded that the relationship of heat-transfer coefficient to other properties of the bed can be understood by using the equation of the form,

$$h = \sqrt{k_m * \rho_m * c * S} \tag{2}$$

where S is the stirring factor accounting for type of bed motion, c is heat capacity of fluidized solids, k_m is the thermal conductivity of quiescent bed and ρ_m is density of quiescent solids.

Di Natale et al. (2009) calculated the heat transfer coefficient at constant surface temperature. With the use of K-type thermocouples, the surface and bulk temperatures were measured to determine the mean and standard deviation of the difference between the wall and bed temperatures. The overall heat transfer coefficient was obtained from the following equation:

$$h = \frac{RI^2}{A(T_w - T_b)} \tag{3}$$

where R is the resistance of the heater cartridge, I is electric current, A is the exchange surface area, T_w is the surface temperature and T_b is the bed temperature.

1.5   Research objectives

The first objective is to study the agglomerates characteristics in a bench-scale MFR (Chapter 3). By changing the rotation speed, the impact of bed mixing will be studied while having a minimal impact on the vapor residence time and the partial pressure. The experimental method of Reyes (2015) will be used to determine the mass of agglomerates, size distribution, amount of liquid trapped, and liquid-solid ratio. The effects of different operating variables such as the bed temperature and the impeller rotation speed in the agglomerate formation will be studied.

The second objective is to study wall-to-bed heat transfer in the MFR while varying the bed material, the particle size, and the MFR scale. The impacts of operating parameters such as mixing speed, bed temperature and vapor flowrate will be studied.

CHAPTER 2

2   Experimental set-up and Methodology

2.1   Equipment

The experiments were performed in a small Mechanically Fluidized Reactor (MFR) which uses a rotating stirrer to agitate a bed of particles, simulating the performance of a conventional fluidized bed without the need for fluidization gas. The reactor vessel is made of stainless steel with a wall thickness of 3.2 mm with additional dimensions provided in Table 2-1.

Table 2-1: Small Mechanically Fluidized Reactor (MFR) sizing details.

Dimension	Units	Sizing
Inner diameter	m	0.1015
Height	m	0.127
Total internal volume	L	1.03
Heat transfer area (Wall)	m^2	0.0405

The flanged tank is equipped with stainless steel lid and a BLUE-GARD® Style 300 Compressed, Non-Asbestos (CNA) gasket. A mixing system is mounted on top of the reactor system, with the driveshaft entering through the center of the reactor flange. A 90 V permanent magnet D.C. gear motor (Leeson Electric Corporation, Grafton, Wisconsin) and a Vari-Drive™ DC Motor Speed Control (KB Electronics, Inc., Coral Springs, FL) are used. The rotational speed range of the model is 0-165 Rotations Per Minute (RPM).

Nitrogen is supplied to the reactor prior to liquid injection and the nitrogen flow is monitored using a flowmeter (Model: MR3A02SVVT, Key Instruments). A pressure relief valve is connected to the system as an additional safety feature in case of pressurization via an exhaust blockage. A 15 psig pressure gauge (ASHCROFT®) is used in this safety arrangement due to its durability as well as chemical and corrosion resistance.

A vertical blade stirrer was used as it was preciously shown to require less power and torque at all aeration rates (Lago et al., 2015). It was also believed to enhance the wall-to-bed heat transfer. The blade stirrer has got two vertical blades as shown in Figure 2-1, where the blade orientation is such that they scrap the wall and draw solids to the center of the bed.
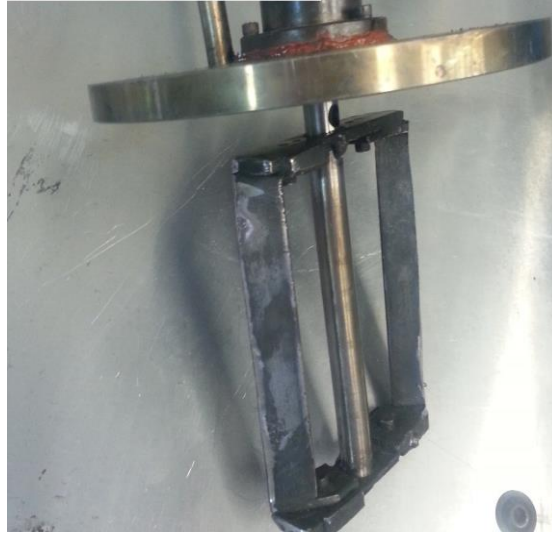
Figure 2-1: Vertical blade stirrer.

A syringe pump (Model: NE-1010, New Era Pump Systems Inc.) was used to inject liquid in batches at various user defined flowrates. A syringe with an inside diameter of 38 mm and 140 ml capacity (Monoject™ Piston syringe, Luer-Lock tip) was selected for liquid injection.
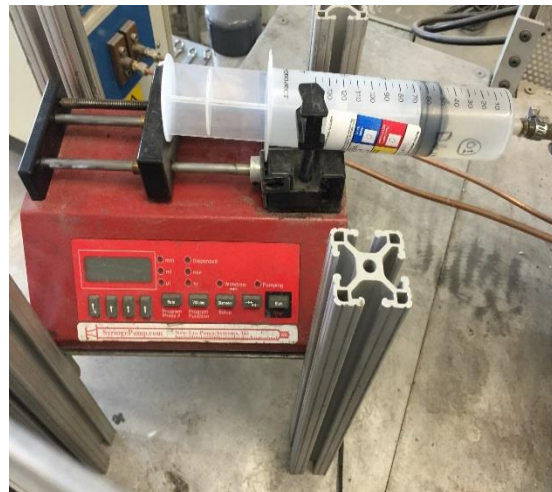
Figure 2-2: Syringe Pump (New Era Pump Systems Inc.) and a partially filled syringe for liquid injection (Monoject™ Piston syringe, Luer-Lock tip).
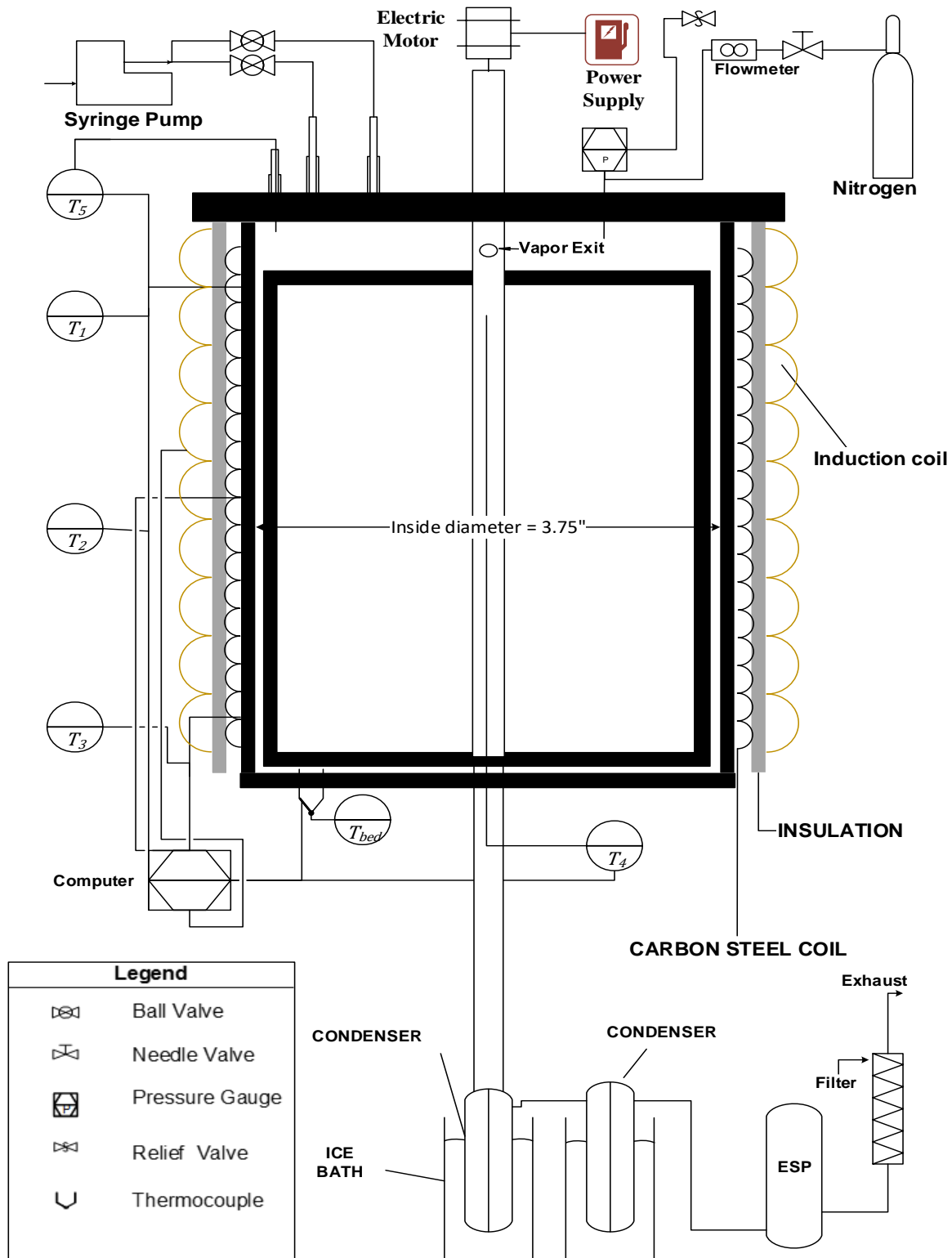
Figure 2-3: Small MFR schematic (reactor is to scale but injection system and condensation train are not to scale).

The MFR was initially equipped with a custom built Induction Heating Machine (IHM-1) (refer to Appendix A- Agglomerate formation study) for performing the experiments related to Chapter 3, while a more powerful Induction Heating Machine (IHM-2) (refer to Appendix B- Heat Transfer study) for carrying out the experiments presented in Chapters 4 and 5.

IHM-1 is 1800 W induction heater (Hannex, Hong Kong, China) which was used to set and maintain the reactor temperature. Temperature readings for the reactor system were acquired at different locations along the wall of the reactor (top, center and bottom regions), in the freeboard region and the bed of the reactor using five K-type thermocouples, two 4-channel thermocouple input (NI-9211 from National Instruments, Austin, TX), and one bus-powered multifunctional DAQ USB Drive (NI USB-6009 from National Instruments, Austin, TX). A program created using the LabWindows™/CVI platform (National Instruments, Austin, TX) acquired the temperature signals. An ON-OFF controller was used to power the induction heating system. The system is equipped with an emergency stop button (BACO) as a safety feature.

IHM-2 is a compact and more powerful heating machine (Superior Induction Company, Pasadena, CA) which can supply power up to 12 kW. It is a medium frequency (30-80 kHz) induction heater. The power for the equipment can be controlled either manually or automatically. In this study, the power supply was controlled manually, making the heating rate control more flexible. Temperature readings were acquired with the same data acquisition assembly and program used when operating with the IHM-1.

The condensing train consisted of two tube condensers in series in an ice-bath, an electrostatic precipitator (ESP) to remove fine droplets of liquid from the gas stream and a gas filter to verify that the ESP is operating effectively.

K-type thermocouples were strategically placed on the wall of the reactor. A carbon steel coil was then wrapped around along the length of the reactor wall, followed by a layer of ceramic fiber insulation, and finally by the induction coil. Due to the high temperature requirement of the experiments, it is important to protect the induction coils from overheating, where the ceramic insulation was used to protect them from any damage.

2.2   Binder Solution

A water, Gum Arabic powder and food dye (Blue No. 1) were used as the particle binder solution. It is important to select the components of the binder solution wisely. Water was selected as a solvent as there is no risk of explosion with air and the vapors exiting the reactor, and they were not harmful if inhaled. Gum Arabic is a polysaccharide that carries a net negative charge (Yang et al., 2012). It is non-toxic, soluble in water and stable up to approximately 200 $^{\circ}$C (Imeson, 2009). The food dye selected for the experiments is neutral or anionic to prevent interactions with the gum that would interfere with the estimation of the dye concentration (refer to Section 2.4.1.2) in the agglomerates (Flury and Flühler, 1994).

Reyes (2015) observed the impacts of changing the binder solution pH (i.e., viscosity) on the agglomeration. Hydrochloric acid was added to the binder solution to adjust its viscosity as the use of strong acid had a great impact in reducing the viscosity when compared to the use of a weak acid (e.g., lactic acid). The pH of the binder solution was measured with Thermo Scientific™ Orion™ 2-Star Benchtop pH Meter. pH values of 3.0 and 1.5 were tested for studying the impact on agglomerate formation. It was observed that for using a pH 1.5, the total reduction in mass of agglomerates was approximately 0.5%. Regardless of the change in the Gum Arabic concentration, the reduction of pH below 1.5 has no considerable effect on the solution viscosity. Pont et al. (2001) reported that the viscosity has a minor effect on the agglomerate stability compared to the impact of capillary forces (i.e., surface tension and wettability).

For each experiment presented in this work, the component concentration in the solution were maintained at constant values. The 93 wt.% of water accounted for the majority of the solution, while Gum Arabic powder with 5 wt.% and Blue No. 1 with 2 wt.% makes up the reminder. The solution was stirred using a Fisher Scientific™ Isotemp™ stirrer to properly dissolve the components in the solution. The binder solution was injected at selected flowrates in the reactor using the syringe pump and syringe arrangement.

2.3   Bed Material

Different bed materials were used for the experiments presented in each Chapter. The particles and their properties have been reported in Table 2-2.

Table 2-2: Details of the bed material used for different Chapters.

Chapter	Reactor	Particle material	Particle size $(d_{p_{sm}})$	Particle density (kg/m^3)	Heat Capacity $(J/kg/K)$	Particle group
3	Small MFR	Silica Sand	190 µm	2650	830	B
4	Small MFR	Silica Sand	190, 300 µm	2650	830	B
5	Small MFR	Silica Sand	600 µm	2650	830	B
	Large MFR	Silica Sand	190 µm	2650	830	B
	Large MFR	Activated Carbon	575 µm	750	1300	B

Silica sand: BELL & MACKENZIE CO. LTD.

Activated Carbon: GC 20 x 50 (General Carbon Corporation, Paterson, NJ)

Figure 2-4, 2-5 are representations of the particle size distribution of the sand used in Small MFR. Figure 2-6 is a representation of the particle size distribution of activated carbon used in Large MFR.
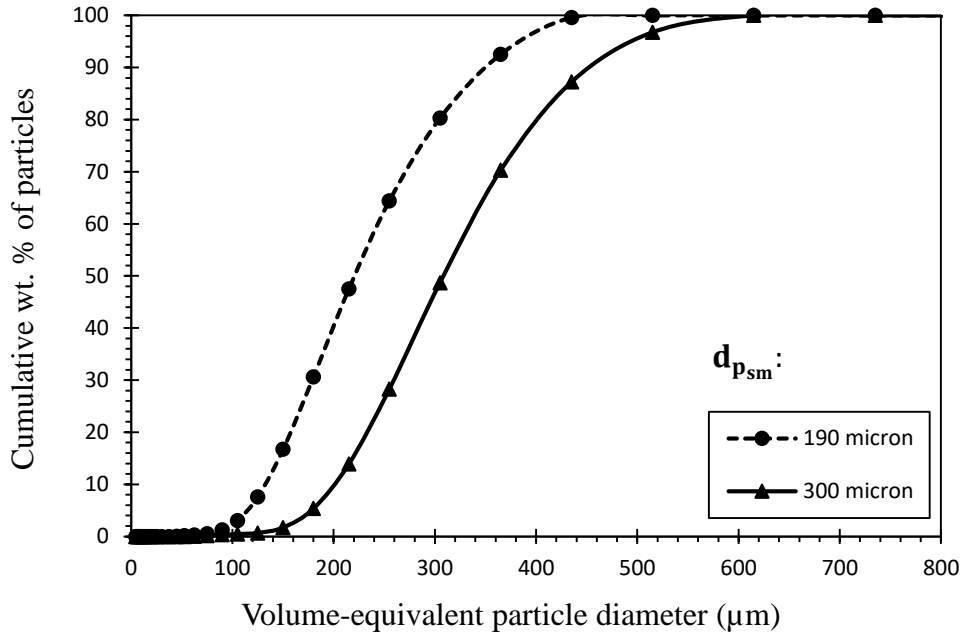
Figure 2-4: Particle size distribution for silica sand ($d_{p_{sm}} = 190, 300\ \mu m$) calculated using a laser diffraction method (HELOS/BF sensor of Sympatec).
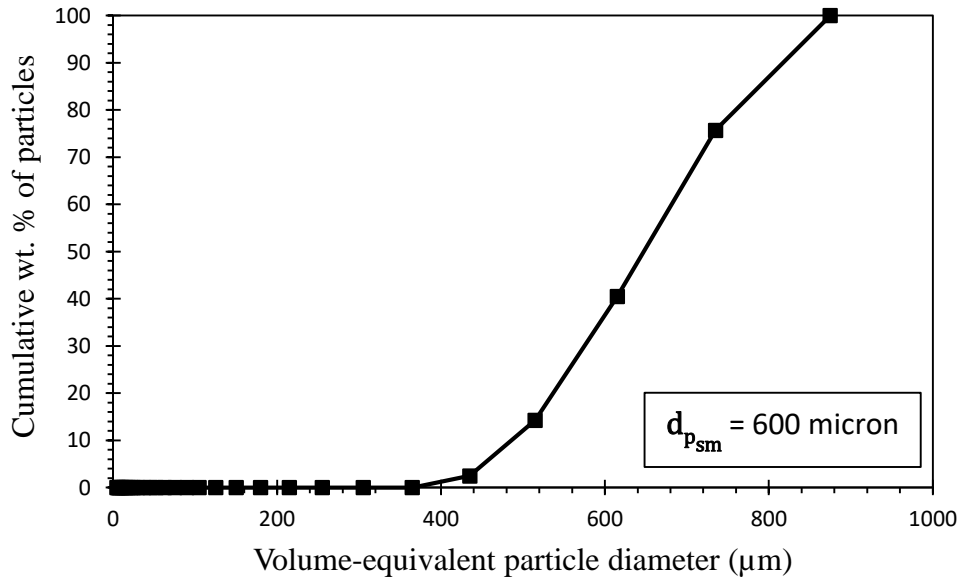
Figure 2-5: Particle size distribution for silica sand ($d_{p_{sm}} = 600\ \mu m$) calculated using a laser diffraction method (HELOS/BF sensor of Sympatec).
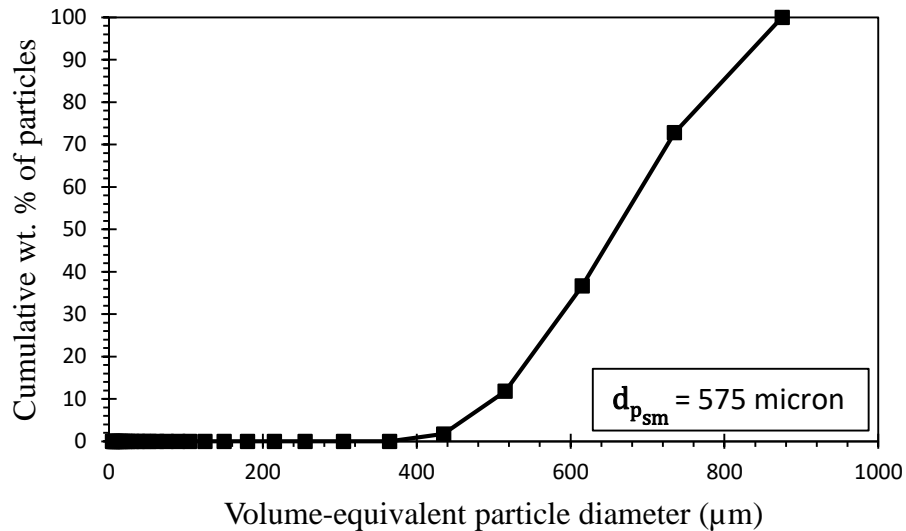
Figure 2- 6: Particle size distribution for activated carbon ($d_{p_{sm}} = 575$ μm) calculated using a laser diffraction method (HELOS/BF sensor of Sympatec).

2.4   Methodology

2.4.1   Agglomerate characterization methods

Each experiment involved the following steps: -

- 400 g of silica sand weighed for each experiment

- Bed temperature (eg., 120 ˚C, 130 ˚C) set for the system

- System is pre-heated using IHM-1 and is allowed to attain steady state

- The Gum Arabic solution is injected in two pulses at a constant flowrate and a pre-determined injection time (e.g., 20 g of liquid solution per pulse at 4 g/min)

- A permanent magnet D.C. gear motor is used to rotate the mixer blades at specified impeller rotation speed (RPM) for each experiment

- Five minutes after the end of the 2nd pulse, the mixing is stopped

- The bed temperature is maintained for some time to completely dry the bed

- The heating is then turned OFF

At the different temperature set-point of the bed and the impeller rotation speed used for each experiment, different number of runs were performed. Either average of a single run or duplicate or triplicate was taken and it is mentioned in the Appendix A- Agglomerate formation study. All the methods used for the characterization of agglomerates are as follows:

2.4.1.1 Agglomerate size distribution

The analysis of the agglomerate size distribution is crucial to understand the behavior in the MFR. With endothermic reactions of the liquid (i.e., thermal cracking), heat transfer within the agglomerates and heat transfer limitations are strongly related to the size and liquid content of these agglomerates. Heat transfer limitations will thus be more pronounced with larger and wetter agglomerates.

Agglomerate formation depends upon various reactor operating conditions. After preheating the reactor bed to the target temperature and the liquid is injected, enough heat is provided for full evaporation. The bed is then cooled down and agglomerates are recovered from the bed by screening. The agglomerates are further classified into:

a) Macro-agglomerates:

Macro-agglomerates have an agglomerate diameter (d_{aggl}) larger than 600 μm. The initial bed material is prescreened to remove particles bigger than 600 μm and therefore, only agglomerates are recovered with a 600 μm screen. Different sieve sizes are then used to classify the macro-agglomerates:

$$d_{aggl} \geq 4000 \ \mu m$$

$$4000 \ \mu m > d_{aggl} \geq 2000 \ \mu m$$

$$2000 \ \mu m > d_{aggl} \geq 1400 \ \mu m$$

$$1400 \ \mu m > d_{aggl} \geq 850 \ \mu m$$

$$850 \ \mu m > d_{aggl} \geq 600 \ \mu m$$

b) Micro-agglomerates

The diameter of micro-agglomerates is 600 µm > d_{aggl} ≥ 355 µm. Thus, in the case of micro-agglomerates some bed particles are mixed with the recovered micro-agglomerates. The amount of sand fines trapped inside the agglomerates is used to estimate the total mass of micro-agglomerates (Reyes, 2015). This estimation requires the following steps:

- Recovery of the micro-agglomerates by screening of the bed material,

- Dissolution of recovered agglomerates in water,

- Centrifugation of the resulting sand/water/dye mix and sampling of the clear liquid to get the dye concentration (refer to Section 2.4.1.2),

- Use of SYMPATEC HELOS/BF (laser diffraction sensor) analysis system for particle size analysis of the samples,

- Assume that all sand particles are equally likely to be trapped in agglomerates and determine the amount of sand trapped in micro-agglomerates from the size distribution of the recovered sand and the size distribution of the initial bed particles,

2.4.1.2   Dye concentration in agglomerates

Both macro as well as the micro-agglomerates go through the same measurement steps to estimate the dye concentration in the agglomerates: -

- A My Weigh® iBalance® iM01™ digital scale with an accuracy of 0.1 mg is used to measure the mass recovered in each sieve size.
- An approximate weight ratio of water to agglomerates of 5:1 ensures complete dissolution of the Gum Arabic and dye and results in an absorbance between 0.1 and 1.
- Solution is centrifuged for 10 min at 4500 rpm in a Thermo Scientific™ Sorvall™ Legend™ X1 Centrifuge to segregate the sand particles from the rest of the solution.
- Absorbance of the clear liquid is measured using the characteristic wavelength corresponding to maximum wavelength of that particular dye (λ_{max}).

- Mass of dye in the agglomerates is determined using Thermo Scientific™ Evolution™ 220 UV-Visible Spectrophotometer.

- The wavelength of maximum absorbance for the dye (Blue No. 1) used for all the experiments in this study is λ_{max} = 630 nm.

- Concentration of the dye in the agglomerates, is estimated using the calibration curve for a particular dye color (Reyes, 2015), shown in Figure 2-6.
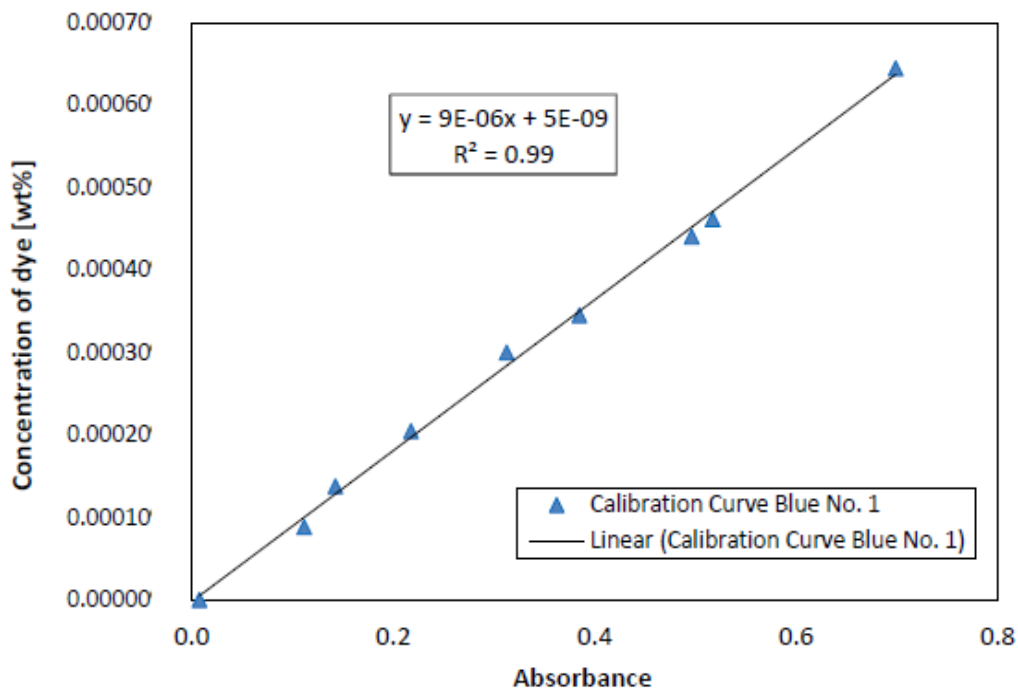
Figure 2-7: Calibration curve for Blue No. 1, λ_{max} = 630 nm (Reyes, 2015).

2.4.1.3   Liquid-to-Solid ratio

A dye was added to the original binder solution to act as a tracer of the liquid originally trapped in the agglomerates, since it remains in the agglomerates once the rest of the liquid has evaporated. From the mass and dye concentration of the dried agglomerates, a mass balance provides the amount of liquid trapped in the agglomerates, and the liquid-to-solid mass ratio.

2.4.1.4   Deposits on wall and mixer blades

Solids deposits formed on the wall and the blades were observed during experiments. As the solids were stuck to wall and the blades, forming a layer of such deposits, this layer had to be scraped off following the experiments. In order to account for the amount of liquid in these deposits, they were collected separately after scratching them off of the wall and, blades, and their total mass was measured. Their dye concentration was measured with the same procedures as for agglomerates (refer to Section 2.4.1.2).

2.4.2   Heat transfer study methodology

A more powerful induction heating machine was used for the heat transfer study experiments (Chapters 4 and 5). The reactor vessel used a carbon steel coil wrapping and a ceramic fiber insulation arrangement similar to that used for experiments performed in Chapter 3. Instead of using the previous induction heating coil (Vibraflame$^®$ extreme temperatures composite cables), it uses a copper coil which needs to be wrapped on top of the ceramic fiber insulation in a strategic manner. The copper coil has its own benefits when compared to the induction heating coils used for previous study. They are less expensive, have a enhanced durability and are readily available. Care should be taken to not pinch the copper coil when plaicng them around the wall as it may render them useless. In such a scenario, where the copper coil cannot be used then a new copper coil cut to the desired length is to be used. Detailed information explaining the control and features of the different induction system is explained in the Appendix -B.

Water was used as the injected liquid for the heat transfer experiments. Each set of experiments had a particular size of silica sand and was studied at varying operating conditions. In the initial set of experiments, bed material with $d_{p_{sm}}$ = 190 µm was used and the impact of the liquid injection flow rate was studied. The bed material was then modified to a $d_{p_{sm}}$ = 300 µm for the next set of experiments and similarly, the flow rate of liquid injection was varied for each run.

A study measuring the overall heat transfer coefficient with an alternating impeller rotation was also performed (clockwise and anti-clockwise manner). The direction of the rotating magnetic field produced by the main and starter windings was modified. Such a change was accomplished

by reversing the polarity of the starter winding. With the help of a rotation controller, the impeller then rotates in clockwise manner for 3 secs, stops for 1 sec and then rotates in an anti-clockwise manner for 3 secs.

2.4.2.1   Steps per run

- 400g of silica sand of a particular size was used for each experiment in small MFR and about 1 kg of different particles used for each experiment in large MFR
- After inserting the top part of the MFR the copper tubing was placed along the walls of the reactor in a strategic manner to minimize the wall temperature fluctuations
- The water supply to the induction heating system is kept at a desired flowrate and the power of the induction heating system is set to 3kW and 6.5kW for small MFR and large MFR respectively.
- Upon starting the induction heating, the carbon steel wires are heated and heat is then transferred from the wires to the bed
- The system is allowed to attain a steady state for approximately 10 to 15 min. Steady state is assumed based on the criteria that the temperature measured at respective location does not deviate more than 1 to 1.5 ˚C.
- Water is injected using a syringe pump at a constant flow rate.
- A permanent magnet D.C. gear motor is used to rotate the mixer blades at constant RPM.
- After setting the desired mixing speed, allow the system to reach steady state for about 7 to 10 min and that measurements are taken after steady state is reached.
- Without shutting off the induction heating, operating conditions (i.e., liquid injection flow rate, mixer rotation) were then modified and system was again allowed to reach steady state before taking the required measurements.

2.4.2.2   Wall-to-bed heat transfer coefficient measurement

The wall-to-bed heat transfer coeffficient were estimated by collecting the temperature measurements using several thermocouples for each experiments performed in small MFR and large MFR.

2.4.2.2.1   Small MFR

The temperature measurements were collected using six thermocouples. The calculations involve the following steps:

- Data was obtained for the bed temperature and the wall temperature using K-type thermocouples having glass insulation

- Wall temperatures were measured at three locations (top, middle and bottom regions) along the wall of the reactor
- The heat inputted to the injected water was estimated by considering the sensible heat for the liquid from the injection temperature to the boiling point, the latent heat of vaporisation, and sensible heat of the vapor from the boiling point to the bed temperature
- The overall heat transfer coefficients obtained from the calculations were then compared to correlated values for gas-solid fluidized beds

2.4.2.2.2   Large MFR

The sizing details for the large MFR are provided in Table 2-3.

Table 2-3: Large Mechanically Fluidized Reactor sizing details.

Dimensions	Units	Large MFR
Inner diameter	m	0.15
Height	m	0.25
Total internal volume	L	4.42
Heat transfer area (Wall)	m^2	0.1178

The temperature measurements were collected using two thermocouples. The calculations involve the following steps:

- Data was obtained for the bed temperature and the wall temperature using K-type thermocouples

- The heat inputted to the injected water was estimated by considering the sensible heat for the liquid from the injection temperature to the boiling point, the latent heat of vaporisation, and sensible heat of the vapor from the boiling point to the bed temperature

- The overall heat transfer coefficients obtained from the calculations were then compared to correlated values for gas-solid fluidized beds, where the superficial gas velocity is estimated based on the volumetric flowrate of steam exiting the large MFR

The calculation assumes that heat losses for the system were negligible. Although this is not accurate, this approximation results in an underestimation of the wall-to-bed heat transfer rate and thus provides a conservative estimate, while also allowing for qualitative comparisons between experiments.

The equations required for the overall heat transfer coefficient estimation are listed as follows:

$$\Delta H_v = C_{P_L} * (100 - 25) + \Delta H_{v_{ref}} + Cp_v * (T_{bed} - 100) \tag{4}$$

$$F_L * \Delta H_v = U * A \left(T_{w_{average}} - T_{bed} \right) - U_L * A_L * (T_{bed} - T_{room}) \tag{5}$$

$$U * A = \frac{F_L * \Delta H_v}{T_{w_{average}} - T_{bed}} \tag{6}$$

Table 2-4: Data for heat transfer coefficient calculation.

Parameter	Units	Value
C_{P_L}	kJ/kg $^\circ$C	4.181
Cp_v	kJ/kg $^\circ$C	2.08
T_{room}	$^\circ$C	25
$\Delta H_{v_{ref}}$	kJ/kg	2257

CHAPTER 3

3 Effects of impeller rotation speed and bed temperature on the properties of agglomerates formed in small MFR

3.1 Introduction

Various studies relating to liquid injection in a fluidized bed have been reviewed in Chapter 1. Good liquid distribution in such systems is essential to achieve the high process efficiencies, operability and reduced environmental footprints that are so important nowadays. Furthermore, product quality is an important factor that is affected, as shown in Chapter 1, by liquid distribution. The formation of agglomerates may or may not be required based on various steps involved in the manufacturing of a given product. In some cases, particle enlargement via agglomeration is desired to improve the in-process product handling or as the final product (Mehta et al., 2005). On the other hand, agglomeration in other processes is undesirable as it can affect the operability of a reactor and the yield of valuable products (Knapper, et al., 2003).

The main focus of this chapter is studying, in a bench scale mechanically fluidized reactor, the relationship between feed flowrate and agglomerate formation, and how the later depends and is affected by bed mixing and temperature. More specifically, the objective is to study the impact of mixer speed and bed temperature on the mass distribution of agglomerates based on their size, liquid-to-solid ratio in the agglomerates and the liquid distribution in agglomerates. The results can be used to estimate the effectiveness of the mechanically fluidized reactor for various applications.

The study is original in terms of its use of induction heating to rapidly heat the bed of a small mechanically fluidized reactor (MFR) and maintain its temperature during liquid injection, where the induction coils are strategically placed on the walls of the reactor vessel to minimize temperature gradients. This approach makes it the first application of the agglomerates formation measurement using solutions of Gum Arabic and dyes in a small MFR unit.

3.2   Materials

Experiments in this chapter were performed using the equipment (**Figure 2-3**) described in Section 2.1.

The binder solution (Gum Arabic) prepared for these experiments had a constant concentration of its constituent ingredients: 93 wt.% of water which accounts for the main portion of the solution, 5 wt.% of Gum Arabic powder, and 2 wt.% of Blue No. 1. The binder solution was prepared separately before each run. Hydrochloric acid was added to the binder solution to adjust the viscosity to 11.25 cp (Model: Brookfield CAP 2000+ Viscometer) at pH = 1.5.

Preliminary experiments in an oven showed that there was significant thermal degradation of the Gum Arabic at temperatures higher than 130°C, as evidenced by a change in color (more information provided in Appendix- A). Experiments were thus conducted at a bed temperature of 130°C or lower. All experiments were performed so that the bed temperature was above the boiling point of water since water was the major constituent of the feed solution. The previous ensures that the liquid will evaporate as soon as it is freed from the agglomerates.

The silica sand used was analyzed with the HELOS/BF sensor of Sympatec before the experimental runs to obtain its Sauter mean diameter. The properties of the bed material used to perform all the experiments related to this Chapter is mentioned in Section 2.3. Figure 3-1 provides the particle size distribution of the sand used in Small MFR.

$d_{p_{sm}}$ = 190 micron
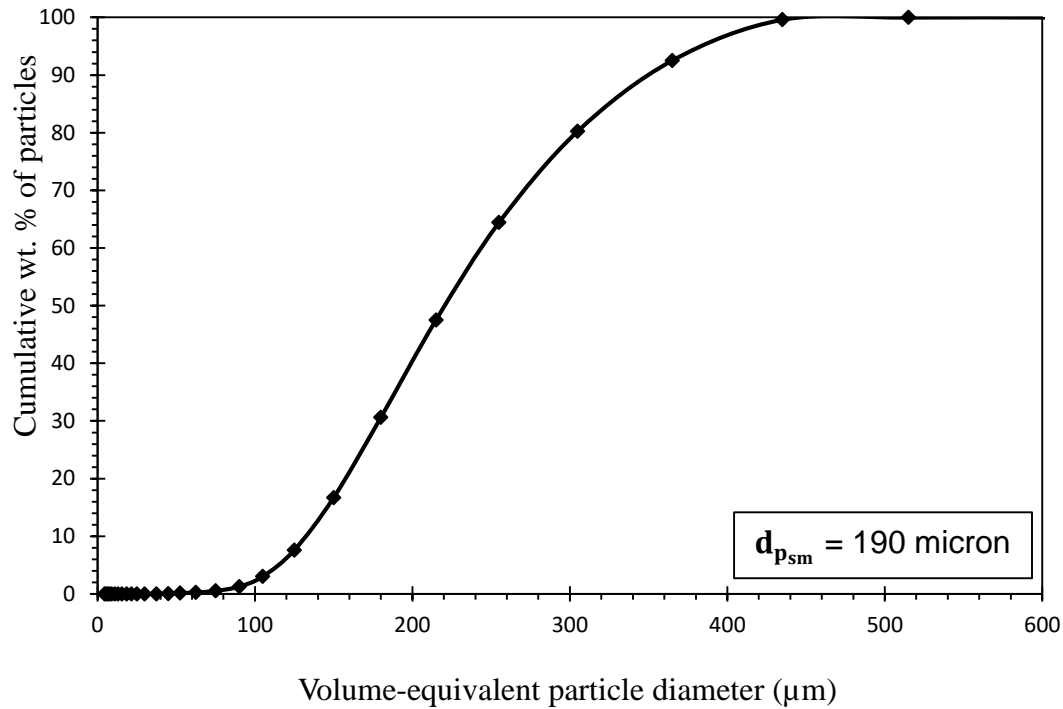
Figure 3-1: Particle size distribution for silica sand calculated using a laser diffraction method (HELOS/BF sensor of Sympatec).

3.3   Method

Silica sand (Group B) is weighed and the binder solution was prepared separately for each experiment. The experimental steps involved in the completion of each experiment are discussed in Section 2.4.

3.4   Results and Discussion

3.4.1   Effect of liquid injection on the bed temperature

Figure 3-2 illustrates that steady state is reached based on the bed temperature profile. Two separate liquid injections are performed, each with a total of 20 ml of water at an injection rate of 4 ml/min. The control of the system bed temperature is generally stable before and after the liquid injections, as observed in the Figure 3-2.
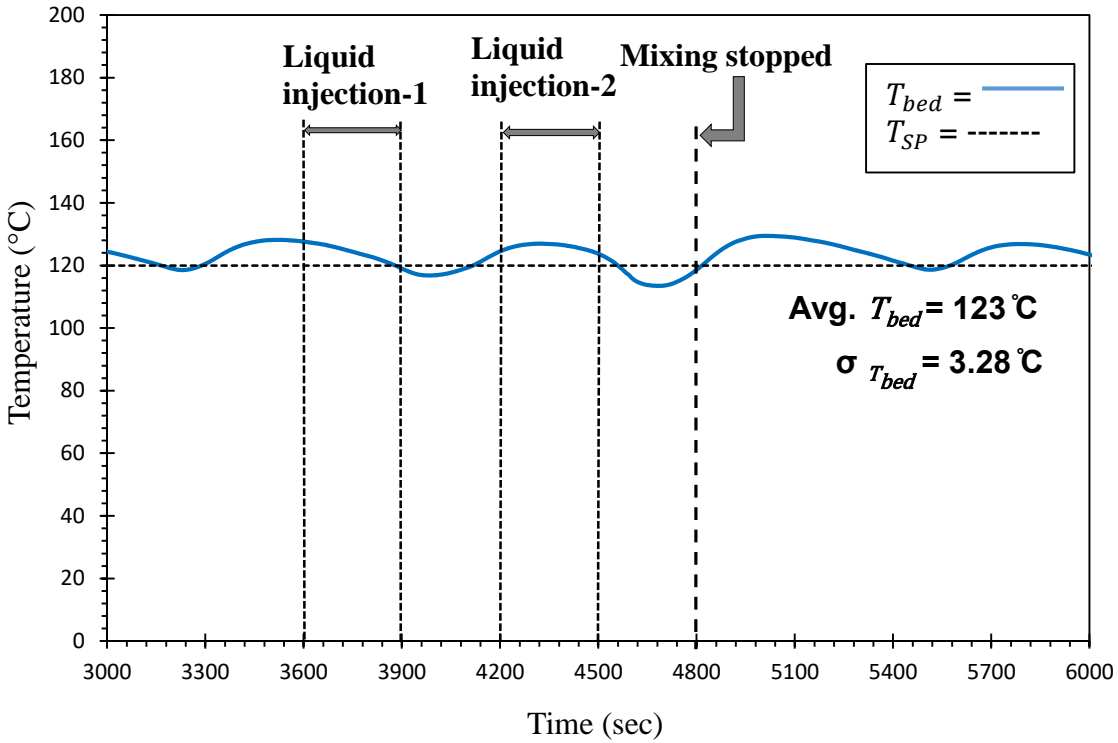
Figure 3-2: Impact of liquid injections (20 ml each) on bed temperature. T$_{SP}$ = 120 °C, Impeller rotation speed = 40 RPM, F$_L$ = 4 ml/min.

The power control for the system is provided in Figure 3-4. The system uses an ON-OFF controller to control the bed temperature. The bed temperature set-point the bed (T_{SP}) for each experiment is decided by the user. During the 'ON' setting, the system heats the wall and the bed of the reactor, and as soon as the temperature of the bed reaches its set-point, the controller turns 'OFF' the induction heating system.
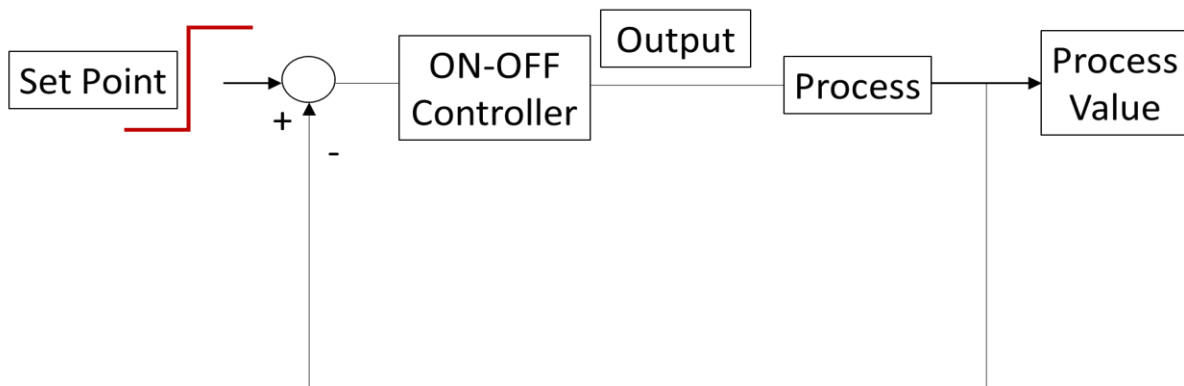
Figure 3- 3: ON-OFF control loop.
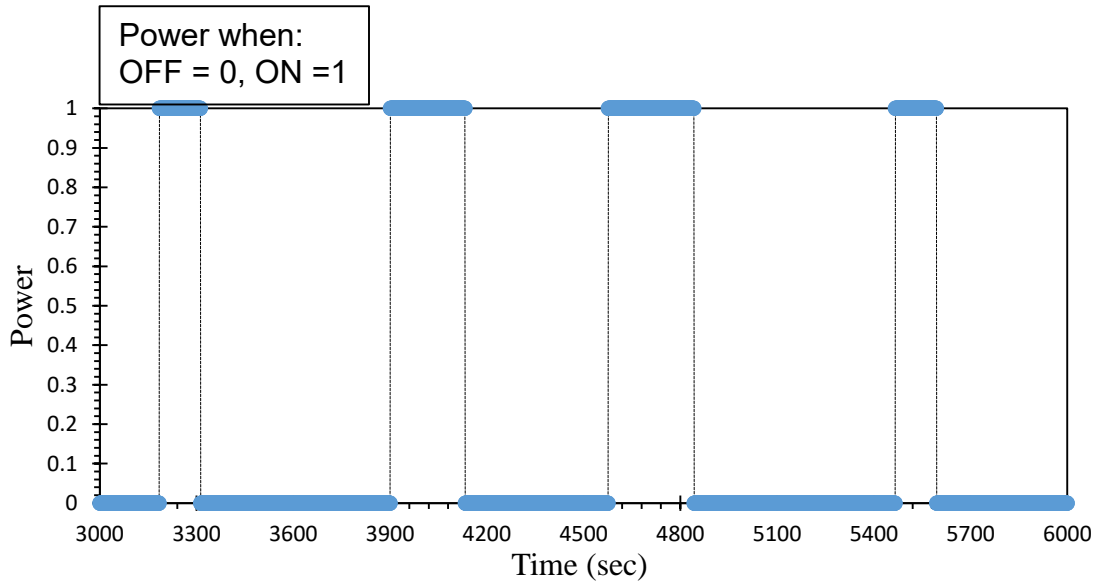
Figure 3-4: Power control of the system for liquid injections (20 ml each). T_{SP} = 120 °C, Impeller rotation speed = 40 RPM, F_L = 4 ml/min.

Figure 3-5 provides the average bed temperatures in the reactor at both studied set-points. Multiple runs at different impeller rotation speed are performed for $T_{SP} = 130$ °C. It can be observed in Figure 3-5 (b), that the average bed temperature results are comparable between runs and for all the impeller rotation speeds that were used.
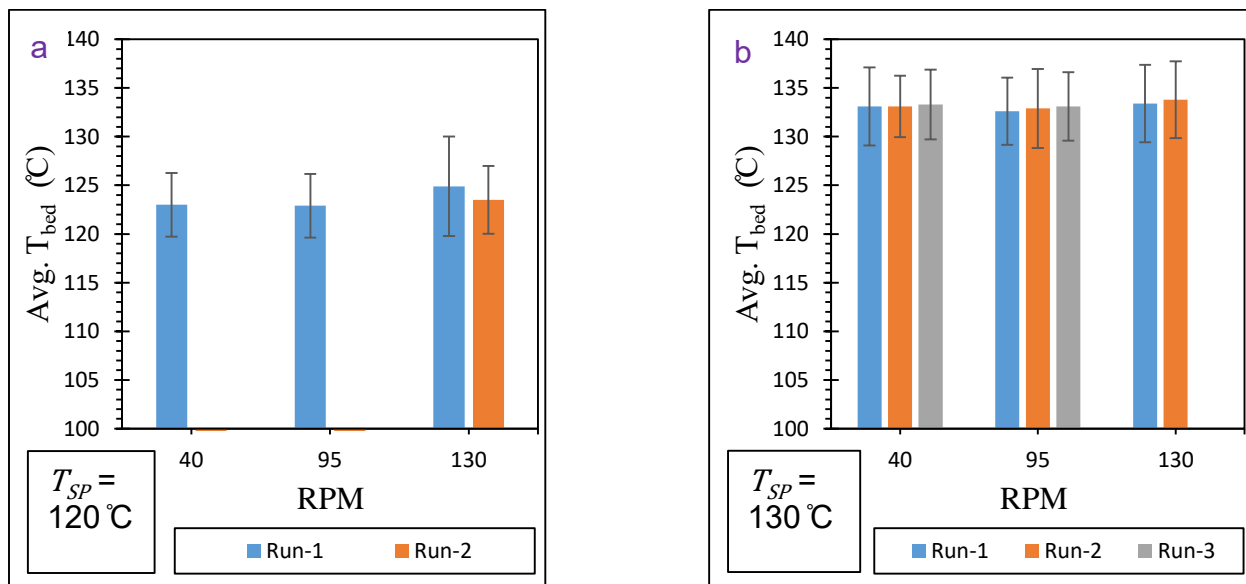
Figure 3-5: Average bed temperature at different impeller rotation speeds between the start of the first liquid injection (3600 s) and the end of mixing (4800 s). Error bars represent the standard deviation between 3600 and 4800 s.

3.4.2 Cumulative wt. % of agglomerates in the bed as a function of agglomerate size

In Figure 3.6, we see that for both bed temperature set-points, increasing the mixing speed reduced the mass of agglomerates. When increasing the impeller rotation speed, agglomerates break more easily, resulting in smaller agglomerates. The small agglomerates survive even when operated at higher mixing speed because the impeller geometry gives an opportunity for the solids to move towards the center of the bed rather than being crushed against the reactor wall.

A mixing speed of 130 rpm increased the amount of small agglomerates which are capable of surviving but at lower rpm's as the movement of blades is slow, larger agglomerates can survive. This trend can be observed for both temperatures. Thus, if the larger agglomerates survive in the reactor (by bypassing the blade), the heat and mass transfer limitations imposed by the large size affect the vaporization of the liquid (Stanlick, 2014).

It can be seen in Figure 3-6, that the total mass of agglomerates is higher at 40 RPM for both studied bed temperatures. There are two possible causes for this: one can be that the initial distribution of the liquid on the particles is not as effective and the agglomerates are wetter, stronger (Weber et al., 2008) or it can be that agglomerate breakup is more effective i.e. there is more shear in the bed. In this case it can be observed that it is due to the second cause.
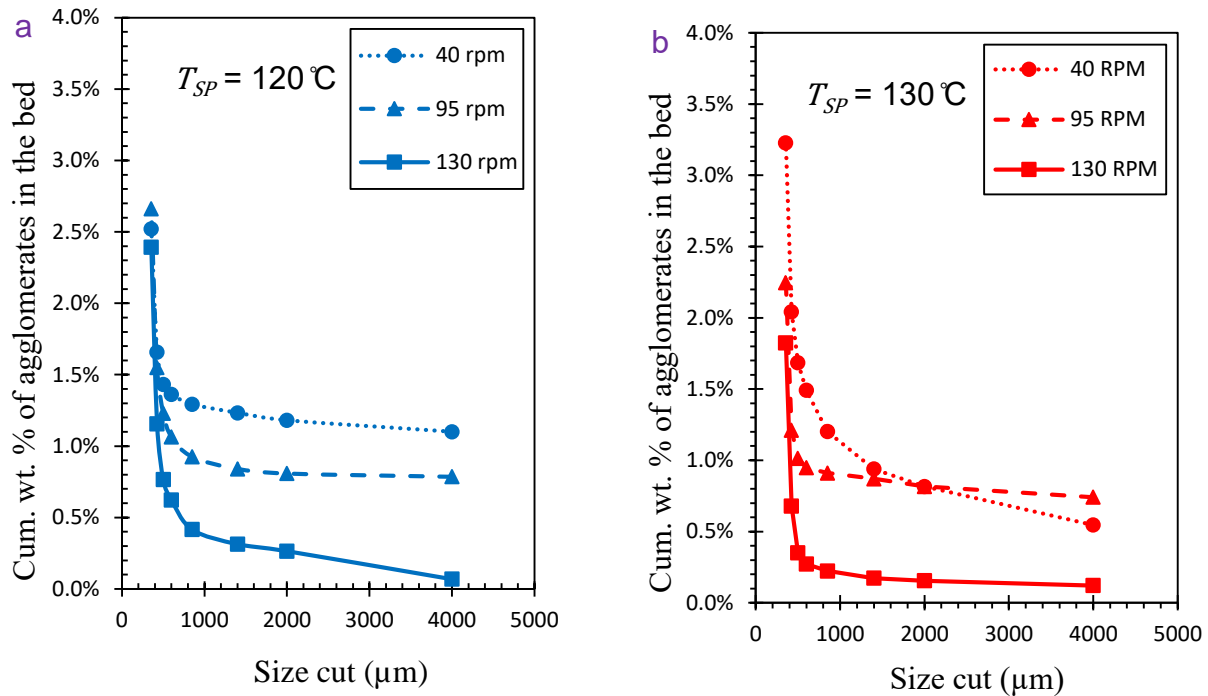
Figure 3-6: Effect of the impeller rotation speed on the formation of agglomerates (mass of agglomerates/mass of bed solids).

3.4.3 Liquid trapped in macro-agglomerates as a function of agglomerate size

Figure 3.7 shows that for both bed temperature set-points, increasing the impeller rotation speed reduced the quantity of liquid trapped in the agglomerates. At a bed temperature of 130°C, shown in Figure 3-7(b), the agglomerates appear to break more easily with the higher impeller rotation speeds of 95 rpm and 130 rpm, and more small agglomerates are formed. This results in a small amount of liquid being trapped in the agglomerates as smaller agglomerates can hold less amount of liquid.

 Increasing the bed temperature set-point also reduced the amount of liquid trapped in macro-agglomerates (i.e., agglomerates larger than 600 µm).
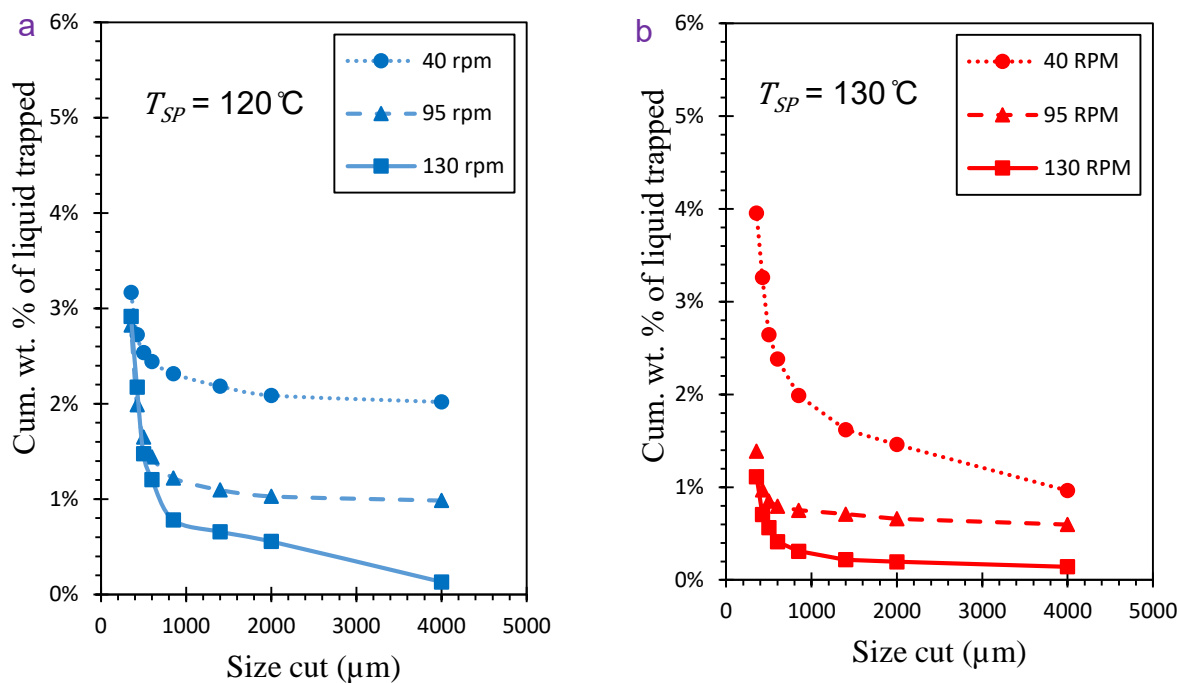
Figure 3-7: Effect of impeller rotation speed on the cumulative liquid trapped in macro-agglomerates.

3.4.4 Effect of bed temperature and impeller rotation speed on the amount of liquid trapped

For the temperature set-point of 120°C, Figure 3-8 shows that there is a small change in the total amount of liquid trapped when increasing impeller rotation speed. At low impeller rotation speed, the agglomerates break up but they also dry quickly. Thus, fragments by shear are still wet and they grow by capturing dry bed particles.

For the higher bed temperature of 130°C, the total liquid trapped in the agglomerates decreases as water evaporates faster at this temperature. At low impeller rotation speed, shear is relatively low and drying by heat conduction is quick. Also, the shear rate cannot compete the rate of drying i.e. there is low break up rate. At lower rpm and higher temperature, Figure 3-8 shows that, the total liquid trapped is more because it causes the outside of the agglomerates to solidify more quickly if they are not broken up quickly, thus trapping more liquid.

The higher bed temperature set-point shows a declining trend in the liquid trapped as we increased the impeller rotation speed. This is because the increased impeller rotation speed breaks up the larger agglomerates, thus reducing the final amount of liquid that was trapped in the agglomerates.
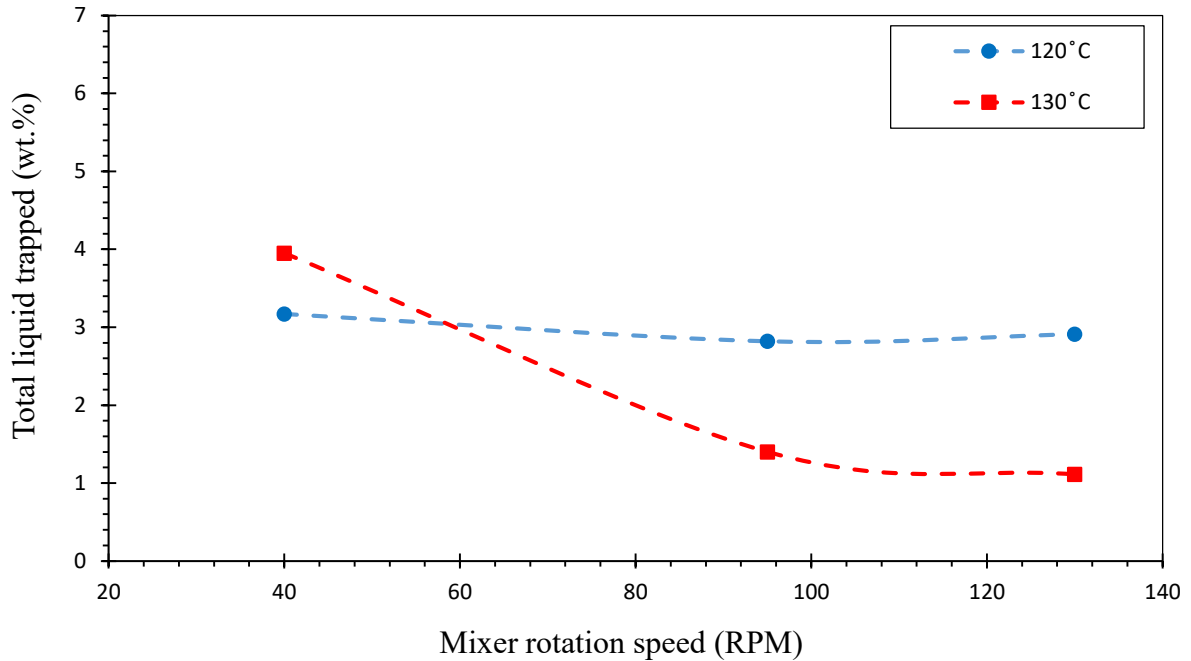
Figure 3-8: Effect of bed temperature and impeller rotation speed on the fraction of injected liquid that is trapped in agglomerates.

3.4.5   Effect of bed temperature and impeller rotation speed on total mass of sand in agglomerates

Figure 3-9 shows that for a bed temperature set point of 120 °C, there was little differences in the total mass of sand in agglomerates at different impeller rotation speed.

On the other hand, for the higher bed temperature (T_{SP} = 130 °C), the total mass of sand in agglomerates decreases with increasing impeller rotation speed. When agglomerates breakup at lower temperature, bed particles stick to the newly exposed, wet surface of the fragments, while

at the higher temperature, the exposed surface dries too quickly to allow for significant capture of the dry bed particles.
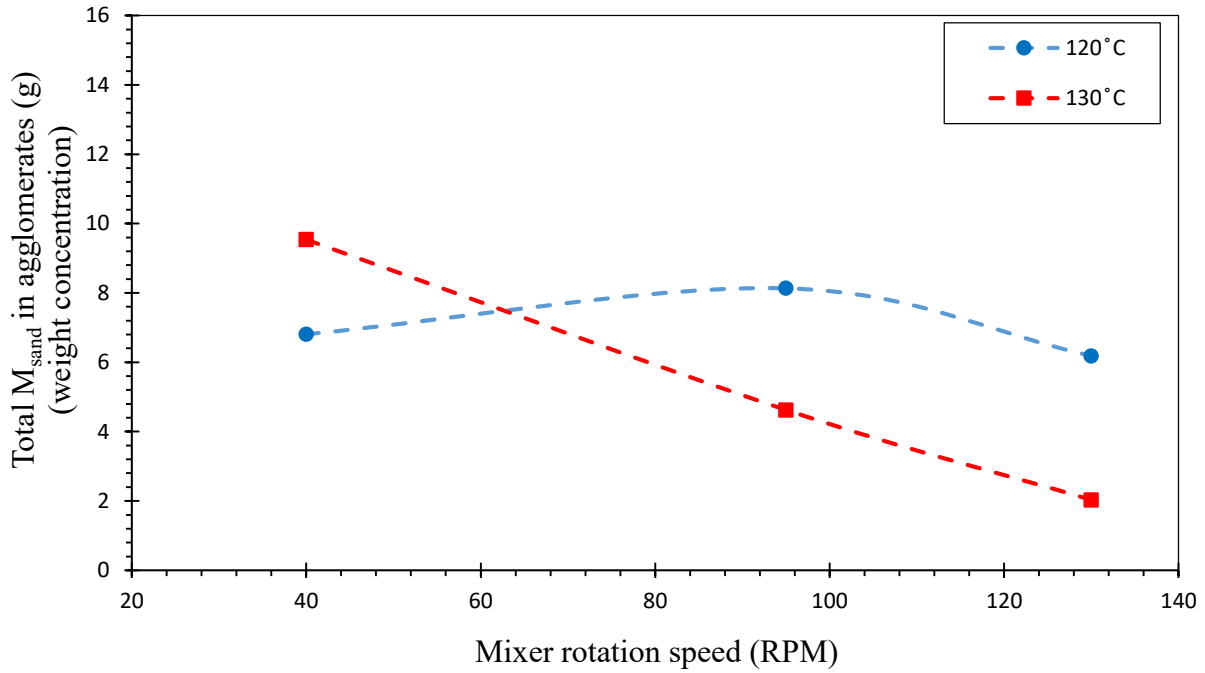
Figure 3-9: Effect of temperature set-point on the mass of sand (M_{sand}) in agglomerates for different impeller rotation speed.

Chapter 4

4 Effect of liquid flow rate and impeller rotation speed on the overall heat transfer coefficient in a Small MFR

4.1 Introduction

The MFR capacity for pyrolysis use is often limited by heat transfer from the hot wall, which is heated by induction, to the bed of biochar particles. The focus of this chapter is thus to investigate the Wall-to-Bed heat transfer in a Mechanically Fluidized Reactor.

Many studies have been conducted on heat transfer from the wall-to-conventional fluidized beds. High heat transfer has been investigated widely in the case of a fluidized bed and there is an increasing demand in the industrial applications such as coating, drying, combustion and ore roasting (Stefanova et al., 2011). It was observed that an increase in the concentration of solids and the density of suspension can lead to an increase in the heat transfer coefficient, and an important factor to determine heat transfer coefficient is convection by means of particles (Basu and Nag, 1987).

Most of the studies performed are relating to the effect of gas velocity on the heat transfer coefficient. Interestingly, different investigators have different take on the effect of the gas velocity. The heat transfer coefficient is larger in some cases with an increase in the gas velocity (Shen et al., 1991) while it was reduced with an increase in the gas velocity due to a reduction in the suspension density (Kee Soo Han et al., 1991). Molerus (1993) observed that the effect of gas velocity on the heat transfer coefficient becomes marginal at operating conditions with similar suspension densities.

Yao et al. (2015) studied the bed-to-wall heat transfer properties of a vertical heat tube in a fluidized bed of FCC particles. It was observed that the measured heat transfer coefficients increase with greater superficial gas velocities. Furthermore, the wall-to-bed heat transfer coefficients were measured at different radial and axial positions with a high accuracy using a specially designed instrument for the study.

The main focus of the present work is to measure the wall-to-bed heat transfer in the Small Mechanically Fluidized Reactor (MFR), and to compare it with heat transfer in conventional fluidized beds. Efforts will then be made to correlate the observed heat transfer coefficients with the correlation given by Molerus et al. (1995), as it allows the prediction of heat transfer coefficient based on its dependence on the superficial velocity of gas. Effects of operating variables such as impeller rotation speed and particle size on the heat transfer coefficient will also be studied.

A study measuring the overall heat transfer coefficient with an alternating impeller rotation as described in Section 2.4.2 was also performed (clockwise and anti-clockwise manner).

Another objective was to study whether the liquid feed rate, and hence the flowrate of vapors through the bed, had an impact on the heat transfer coefficient values, as it does with conventional fluidized beds. Lastly, experiments will use different particle sizes of silica sand to study its impact.

The study is original in terms of its use of induction heating to rapidly heat the bed of a small mechanically fluidized reactor (MFR) and maintain its temperature during liquid injection, where copper coils are strategically placed on the walls of the reactor vessel to minimize temperature gradients. This approach makes it the first study on heat transfer coefficient measurement in a small MFR unit.

4.2   Material

Experiments relating to this chapter are all performed using the equipment described in Section 2.1. The properties of the bed material in this Chapter are provided in Section 2.3. Silica sand used for performing all the experiments is analyzed before using it for the experimental purpose in order to obtain the Sauter mean diameter. Figure 4-1 is a representation of the particle size distribution of the sand used in Small MFR.
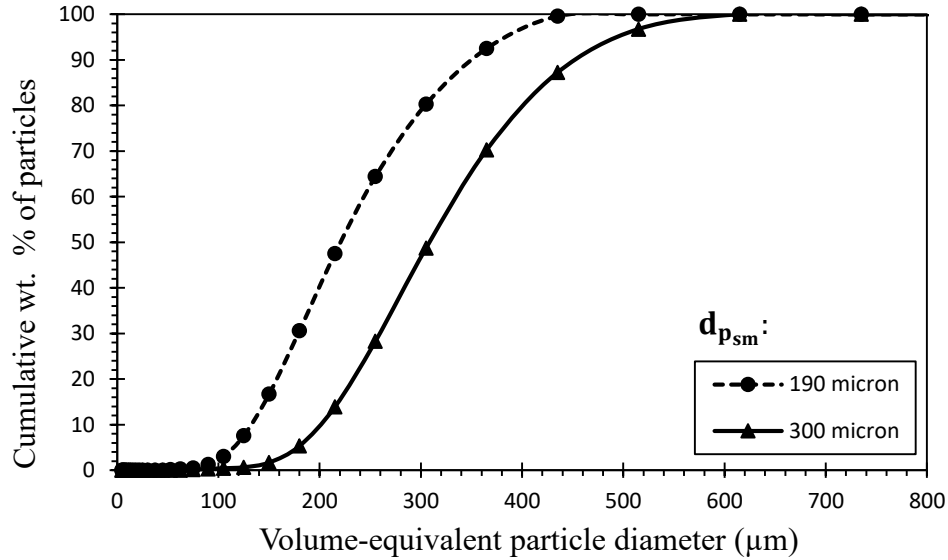
Figure 4-1: Particle size distribution for silica sand calculated using a laser diffraction method (HELOS/BF sensor of Sympatec).

4.3   Method

The experimental procedure followed has been previously discussed in Section 2.4.2.1. The wall-to-bed heat transfer coefficient measurement has been described in Section 2.4.2.2. The studies presented in this work were performed using two particle sizes in the Small Mechanically Fluidized Reactor (MFR). The sizing details of the studied reactor is provided in Table 4-1. In this chapter, superficial steam velocities reported are calculated at the freeboard conditions just above the bed temperature.

Table 4-1: The Small MFR reactor vessel sizing details.

Dimensions	Units	Small MFR
Inner diameter	m	0.1015
Height	m	0.127
Total internal volume	L	1.03
Heat transfer area (Wall)	m^2	0.0405

Equations required to estimate the overall heat transfer coefficient have been previously provided in Section 2.4.2.2. Heat transfer coefficient obtained for each experimental conditions are then compared with correlated vales for standard fluidized beds, based on the following correlation by Molerus et al. (1995), which is stuitable for the type of particles used in this study, based on the Archimedes number ($Ar = d_p{}^3(\rho_p - \rho_g)\rho_g g/\mu^2$) where $10^2 < Ar < 10^5$: $\qquad$ (7)

$$\frac{hl_l}{k_g} = \frac{0.125*(1-\varepsilon_{mf})(1+33.3\{\sqrt[3]{[\frac{u-u_{mf}}{u_{mf}}]^3}\,\sqrt[3]{(\rho_p c_p/k_g g)}(u-u_{mf})\}^{-1})^{-1}}{1+\left(\frac{k_g}{2c_p}\mu\right)\{1+0.28(1-\varepsilon_{mf})^2\left[\frac{\rho_g}{\rho_p-\rho_g}\right]^{0.5}[\sqrt[3]{\left(\frac{\rho_p c_p}{k_g g}\right)}(u-u_{mf})]^2\frac{u_{mf}}{(u-u_{mf})}\}}$$

$$+0.165Pr^{\frac{1}{3}}(\frac{\rho_g}{\rho_p-\rho_g})^{\frac{1}{3}}[1+0.05\left(\frac{u-u_{mf}}{u_{mf}}\right)^{-1}]^{-1} \qquad (8)$$

4.4   Results and Discussion

4.4.1   Experiments with smaller particles ($d_{p_{sm}}$ = 190 µm)

Experiments were first performed using the sand particles (Group B) with properties provided in Table 4-2 and using non-alternating rotation for the impeller.

Table 4-2: Properties of the smaller particles ($d_{p_{sm}}$ = 190 µm).

Particle material	Particle Sauter mean diameter ($d_{p_{sm}}$)	Particle density (kg/m³)	Heat Capacity (J/kg/K)
Silica Sand	190 µm	2650	830

Runs were performed with different flow rates of liquid injection and while varying the impeller rotation speeds. Following the injection of several liquid pulses using a syringe pump-syringe assembly (refer to **Figure 2-2**), the system was allowed to reach steady state. Figure 4-2 shows an example of steady state being reached at gradually higher mixing speeds during liquid injection at flowrate corresponding to a superficial steam velocity of 43 mm/s. The power

42

supplied (3 kW) from the IHM-2 (detailed in Appendix B) is continuous and results in elevated temperatures in the reactor bed and wall. The wall temperature was measured at three separate locations and reached temperatures of approximately 600°C relatively quickly (approx. 45 mins when starting at room temperature) and the system was allowed to reach steady state before liquid injection was initiated.

At a time of 4200 s in Figure 4-2, the liquid injection was initiated with no mixing and an injection rate of 5 ml/min, corresponding to a steam velocity of approximately 43 mm/s (assuming steam properties at 623°C). The system requires sufficient time to reach steady state when there is no mixing, as evident from the Figure 4-2. When the temperature measured at different locations on the wall and the bed temperature show a deviation of not more than $\pm$ 1°C for approximately 7 to 10 min, it was then considered to be steady state. A new mixing speed was then applied at approximately 7700 s, while maintaining the liquid injection flow rate. The system was then again allowed to reach steady state. It can be seen that steady state was reached more rapidly at the impeller rotation speed of 22 rpm when compared to 0 rpm. The previous method was then followed for different impeller rotation speeds using the same liquid injection flow rate.
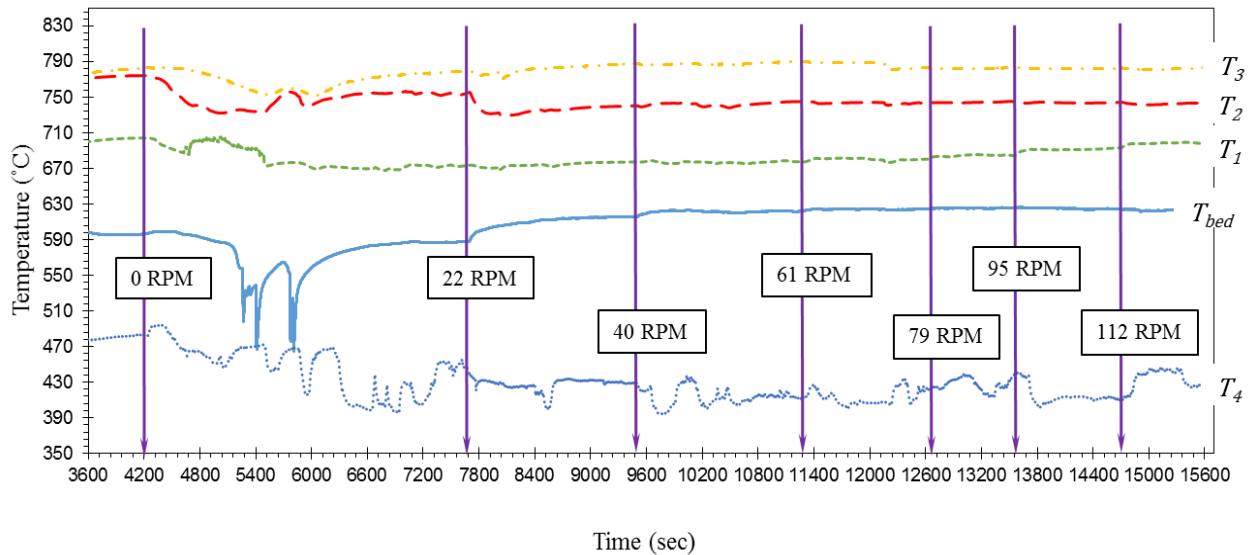
Figure 4-2: Bed and wall temperatures at an superficial steam velocity of 43 mm/s and different mixer speed using Silica sand $d_{p_{sm}}$ = 190 μm.

Figure 4-3 presents the effect mixing speed and the superficial steam velocity on the bed temperature. The bed temperature was reduced by more than 100 ℃ as the superficial steam velocity is increased from 43 mm/s to 112 mm/s. The previous trend was expected as the increased heat requirements to evaporate the higher liquid injection resulted in a reduction of the bed temperature. It was also observed that there was a small increase in the bed temperature with increasing impeller rotation speed, resulting in better liquid-solid contact and an increased heat transfer inside the reactor.
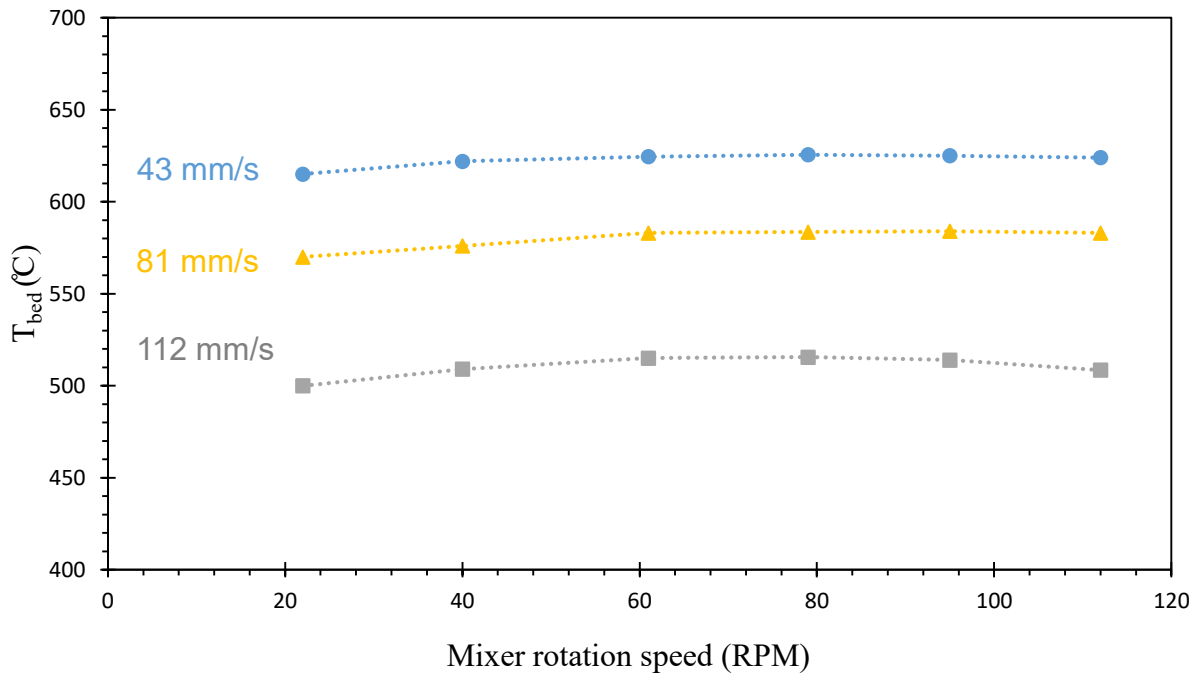
Figure 4-3: Effect of mixing speed on the measured bed temperature for superficial steam velocities in Small MFR. Silica sand $d_{p_{sm}}$ = 190 µm.

4.4.2 Experiments with Small MFR and particles with $d_{p_{sm}}$ = 300 μm

Experiments were then performed using larger sand particles (Group B) with properties the provided in Table 4-3 and using non-alternating rotation for the impeller.

Table 4-3: Properties of the bed material ($d_{p_{sm}}$ = 300 μm).

Particle material	Particle Sauter mean diameter ($d_{p_{sm}}$)	Particle density (kg/m³)	Heat Capacity (J/kg/K)
Silica Sand	300 μm	2650	830

Similar to the smaller particles, Figure 4-4 demonstrates that the bed temperature is also reduced for the larger particles when increasing the superficial steam velocity (i.e., liquid injection flow rate).

It can be because at high steam superficial velocities and the increase in the rpm, the gases and vapors travel to the bottom of the bed faster. The increased liquid injection flow rate affects the cooling of the bed as the latent heat requirement increases. For the superficial steam velocities of 41 mm/s and 79 mm/s, the impeller rotation speed affects the wall-to-bed heat transfer. At the superficial steam velocity of 111 mm/s, the bed temperature decreases slightly with an increase in the rpm and is the only exception to the trend seen so far.

Figure 4-4: Effect of mixing speed on the measured bed temperature for superficial steam velocities in Small MFR. Silica sand $d_{p_{sm}}$ = 300 μm.

4.4.3 Comparison of the overall heat transfer coefficient with different particle sizes

Figure 4-5 shows that the maximum superficial steam velocity corresponds to the highest heat transfer coefficient between the wall and bed. This indicates that a better aeration of the bed enhances the wall-to-bed heat transfer. The heat transfer coefficient also increases with higher rotation speeds, especially at higher superficial steam velocities. An exception is at very high impeller speeds and the highest superficial steam velocity, for which there is a decrease in heat transfer after exceeding the maximum value (at a RPM of approximately 80). It is suspected that at very high impeller rotation speeds, centrifugal forces mean that a thin layer of nearly stationary bed material forms along the wall of the reactor, impairing heat transfer.

The overall heat transfer coefficient values for the smaller particle size ($d_{p_{sm}}$ = 190 µm) are generally lower when compared to the bigger sand particle size ($d_{p_{sm}}$ = 300 µm) for the studied impeller rotation speeds. In the case of higher flowrates of liquid, there is formation of much stronger and wetter agglomerates inside of the reactor, thus, more time is needed to break the agglomerates and dissipate the liquid from the agglomerates.
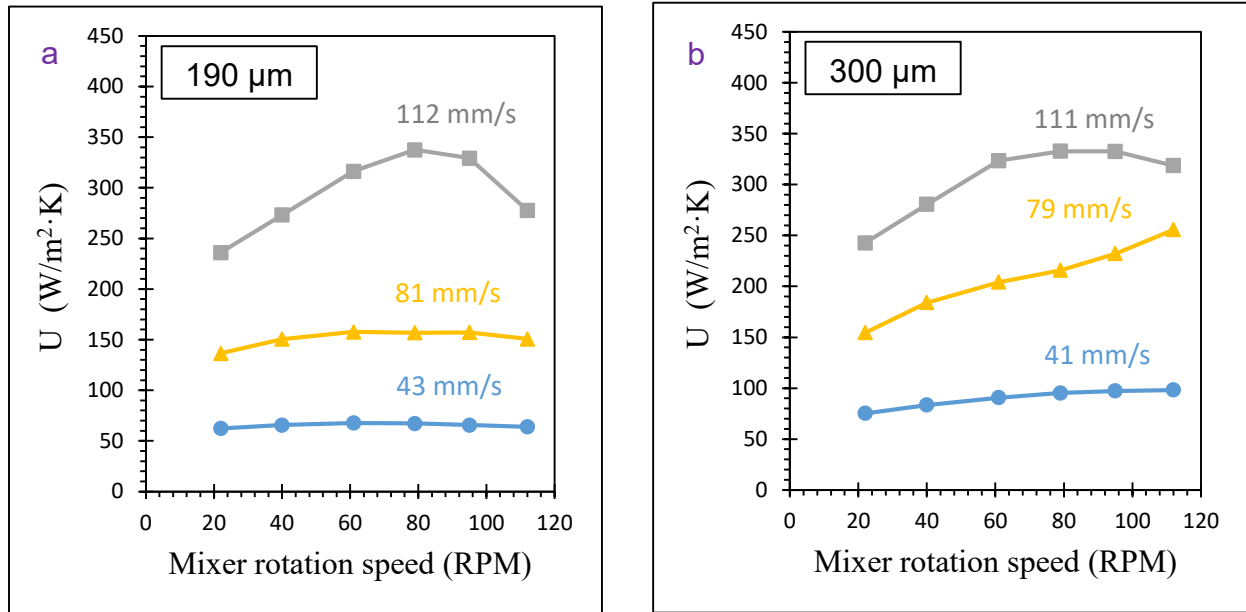
Figure 4-5: Overall heat transfer coefficient for two different particle size of silica sand at different impeller rotation speeds and superficial steam velocities in Small MFR.

Table 4-4 and Table 4-5 provides the overall heat transfer coefficient obtained with the Small MFR for both studied particle sizes. The overall heat transfer coefficient increased with at the higher superficial steam velocity for both particle sizes. A more interesting analysis of the experimental results is obtained by comparing with the Molerus correlation. It is observed that the Molerus correlation for conventional fluidized beds provides comparable predictions for the studied 300 µm silica sand.

Table 4-4: Comparison of the average overall heat transfer coefficient with that obtained from Molerus correlation for Silica sand $d_{p_{sm}}$ = 190 μm in Small MFR.

Flow rate (ml/min)	Superficial steam velocity (mm/s)	$U_{average}$ for studied RPM (W/m²·K)	U from correlation (W/m²·K)	U_{max} (W/m²·K)	$U_{max}/U_{correlation}$ (-)
5	43	66	142	68	0.48
10	81	152	344	158	0.46
15	112	295	428	338	0.79

Table 4-5: Comparison of the average overall heat transfer coefficient with that obtained from Molerus correlation for Silica sand $d_{p_{sm}}$ = 300 μm in Small MFR.

Flow rate (ml/min)	Superficial steam velocity (mm/s)	$U_{average}$ for studied RPM (W/m²·K)	U from correlation (W/m²·K)	U_{max} (W/m²·K)	$U_{max}/U_{correlation}$ (-)
5	41	90	73	98	1.34
10	79	208	329	256	0.78
15	111	305	423	333	0.79

In Figure 4-6, U (300 µm)/U (190 µm) indicate the ratio for the overall heat transfer coefficient values for two different particle sizes. It is observed that the Molerus correlation for conventional fluidized beds accounts well for the impact of bed particle size on the measured overall heat transfer coefficient values for the two highest liquid injection flow rates. At the lowest liquid flowrate, there would not be enough steam generated to fluidize the bed. The minimum fluidization velocity is obtained using the Richardson and S. Jeronimo (1979) correlation. For

particles with $d_{p_{sm}} = 300$ µm, in the case of lowest liquid flow rate (i.e., at 5 ml/min) the superficial steam velocity is 41mm/s, while the minimum fluidization velocity is 47 mm/s.
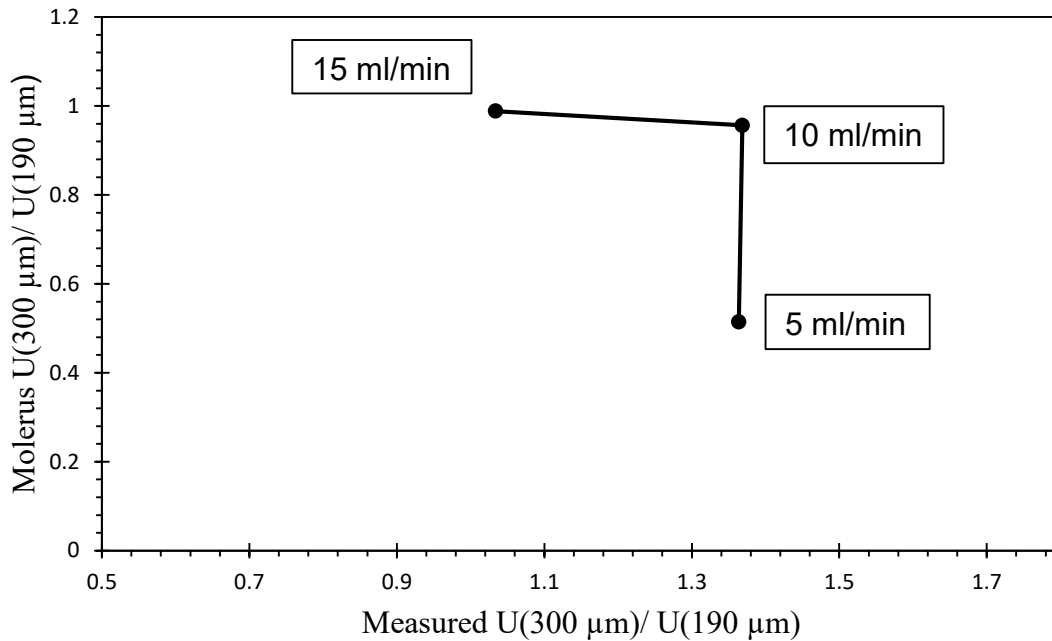
Figure 4-6: Molerus U (300 µm)/U (190 µm) vs. Measured U (300 µm)/U (190 µm).

4.4.4   Small MFR with alternating rotation for the impeller

Experiments were performed using the sand with properties provided in Table 4-6. Runs were performed with different flow rates of liquid injection and while varying the impeller rotation speeds. Following the injection of several liquid pulses using a syringe pump-syringe assembly (refer to Figure 2-2), the system is allowed to reach steady state. The impeller rotates in clockwise manner for 3 secs, stops for 1 sec and then rotates in an anti-clockwise manner for 3secs.

Table 4-6: Properties of the bed material ($d_{p_{sm}} = 190$ µm).

Particle material	Particle size ($d_{p_{sm}}$)	Particle density (kg/m³)	Heat Capacity (J/kg/K)
Silica Sand	190 µm	2650	830

Figure 4-7 presents the effect of the mixing speed and the superficial steam velocity on the bed temperature. The temperature of the bed falls as the superficial steam velocity is increased from 40 mm/s to 104 mm/s. The previous trend was expected as the increased heat requirements to evaporate the higher liquid injection resulted in a reduction of the bed temperature.
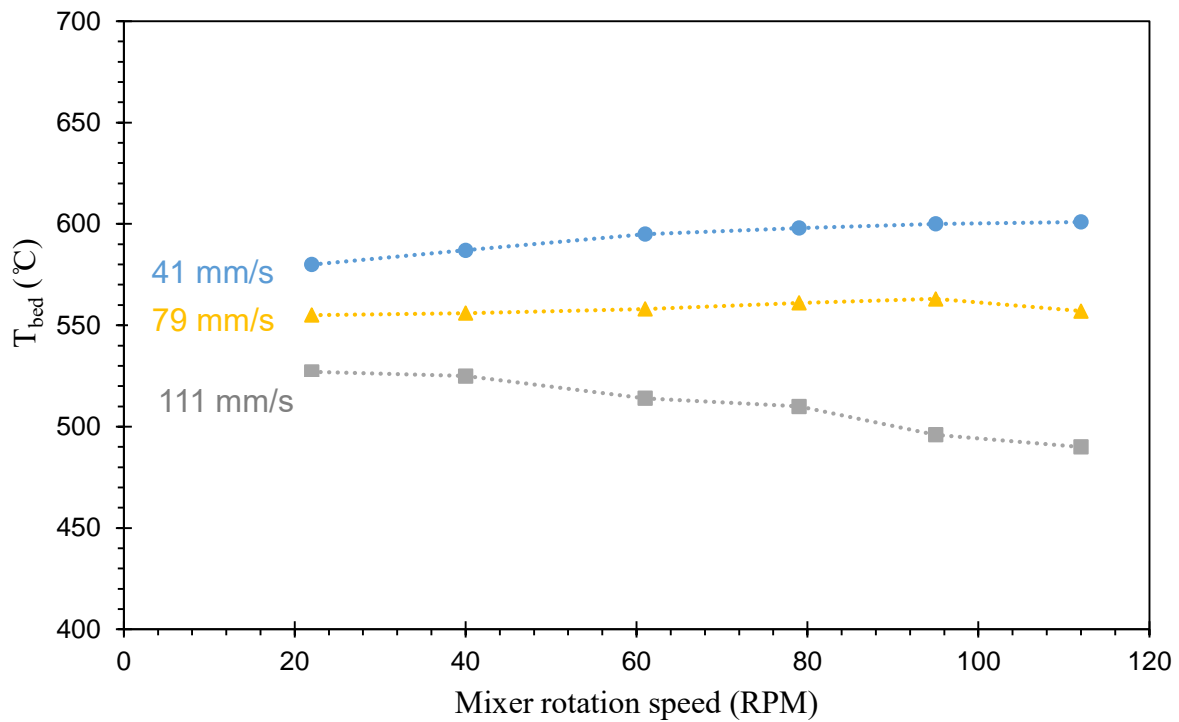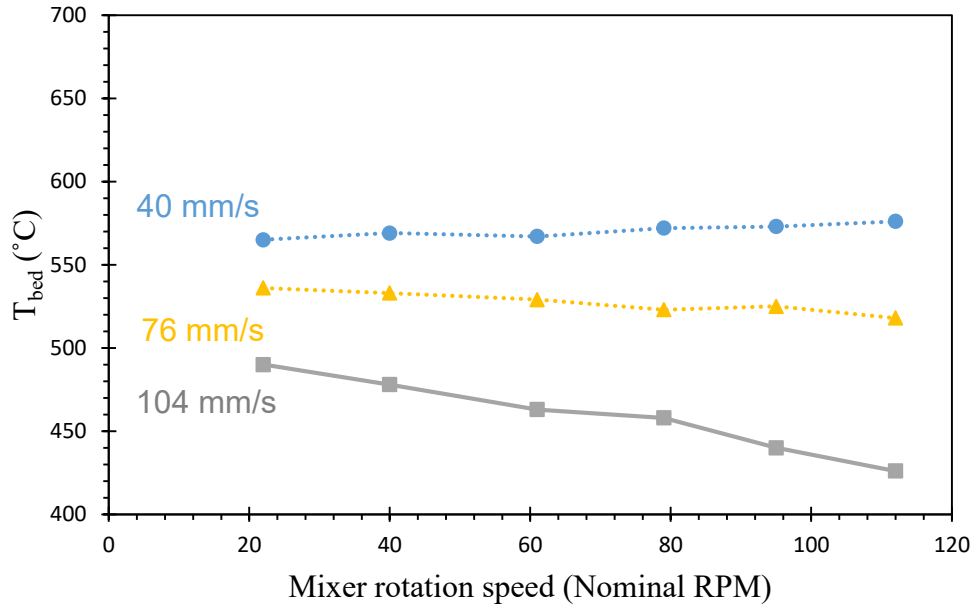

Figure 4-7: Effect of mixing speed on the measured bed temperature for superficial steam velocities in Small MFR with alternating effect of the impeller. Silica sand $d_{p_{sm}}$ = 190 μm.

Figure 4-8 shows that the maximum superficial steam velocity corresponds to the highest heat transfer coefficient between the wall and bed. This indicates that a better aeration of the bed enhanced the wall-to-bed heat transfer.

The heat transfer coefficients generally increased with increasing rotation speed, especially at higher superficial steam velocities. An exception to the trend is seen at the superficial steam velocity (76 mm/s) beyond impeller rotation speed of 95 rpm (nominal), for which there is a decrease in heat transfer as is evident in Figure 4-8. It is suspected that at very high impeller rotation speeds (using non-alternating impeller rotation), centrifugal forces result in a thin layer of nearly stationary bed material forms along the wall of the reactor, impairing heat transfer. It is believed that the alternating effect of the impeller rotation reduced this layer of stationary solids

which is formed (which otherwise would have resulted in lower heat transfer coefficients) as the impeller rotates in both directions.
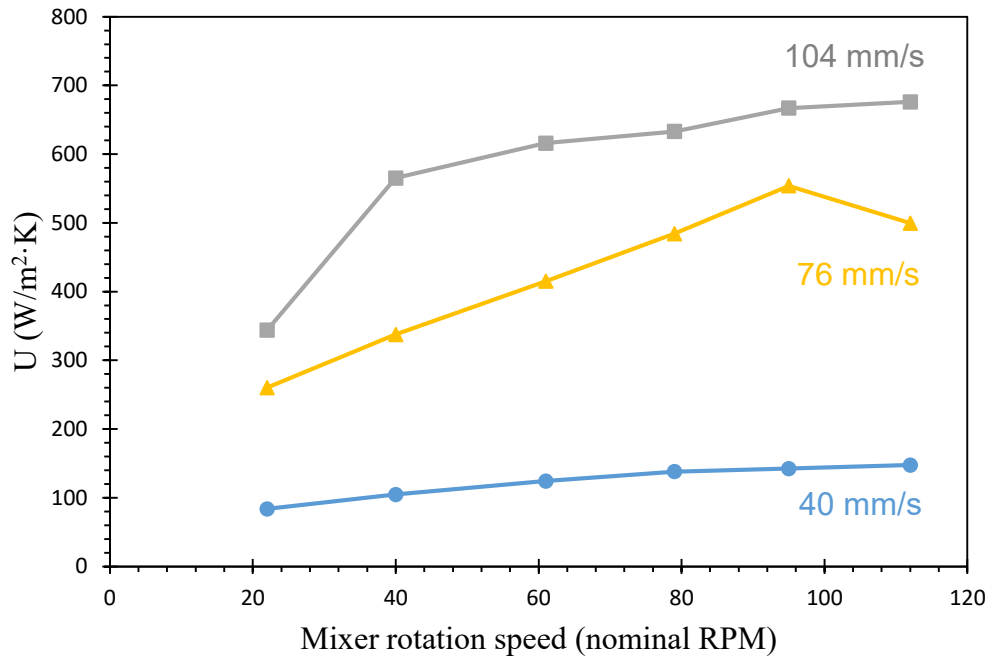
Figure 4-8: Overall heat transfer coefficient for different mixer speeds and superficial steam velocities in Small MFR with alternating effect of the impeller. Silica sand $d_{p_{sm}}$ = 190 μm.

Table 4-7 provides the overall heat transfer coefficient obtained with the Small MFR. The overall heat transfer coefficient increased with at higher superficial steam velocities for both particle sizes. A more interesting analysis of the experimental results is obtained by comparing with the Molerus correlation. The overall heat transfer coefficient obtained from the experiment is higher at higher superficial steam velocities than the values obtained from the Molerus correlation.

Table 4-7: Comparison of the average overall heat transfer coefficient with that obtained from Molerus correlation for Silica sand $d_{p_{sm}}$ = 190 μm in Small MFR with alternating effect of the impeller.

Flow rate (ml/min)	Superficial steam velocity (mm/s)	$U_{average}$ for studied RPM (W/m²·K)	U from correlation (W/m²·K)	U_{max} (W/m²·K)	$U_{max}/U_{correlation}$ (-)
5	40	123	118	148	1.25
10	76	425	300	554	1.85
15	104	584	387	676	1.75

Table 4-8 compares the effect of alternating and non-alternating impeller rotation in Small MFR. It can be seen that, with an increase in the superficial steam velocity there is an increase in the overall heat transfer in Small MFR for both impeller rotation methods. Nonetheless, the overall heat transfer coefficient is significantly greater in the case of the alternating rotation of the impeller. This can be caused due to the rotation of the impeller in an alternating manner which likely reduces the formation of the solid layer along the wall of the reactor, improving the wall-to-bed heat transfer.

Table 4-8: Comparison of the average overall heat transfer coefficient for particles of same size and the rotation of impeller in two different manners.

Flow rate (ml/min)	Superficial steam velocity (mm/s)	$U_{average}$ for studied RPM (W/m²·K)		Flow rate (ml/min)	Superficial steam velocity (mm/s)
		Small MFR (Non-alternating impeller rotation)	Small MFR (Alternating impeller rotation)		
		Sand size = 190 µm	Sand size = 190 µm		
5	43	66	123	5	40
10	81	152	425	10	76
15	112	295	584	15	104

The increase in the heat transfer coefficient for alternating impeller rotation is presented in Figure 4-9. The increased heat transfer coefficient, starts with the onset of fluidization, when the superficial steam velocities (v_g) in excess of the minimum fluidization velocity (U_{mf}). The minimum fluidization velocities (presented in Table 4-9) obtained from the correlation by Wen and Yu (1966) help us obtain the velocity ratio (v_g /U_{mf}). The velocity ratio appropriately shows the dependence of the overall heat transfer coefficient on the superficial steam velocity.

Table 4-9: Minimum fluidization velocities for particles of same size and the rotation of impeller in two different manners.

Superficial steam velocity (mm/s)	Minimum fluidization velocity (mm/s)		Superficial steam velocity (mm/s)
	Small MFR (Non-alternating impeller rotation)	Small MFR (Alternating impeller rotation)	
43	16	17	40
81	17	18	76
112	19	20	104
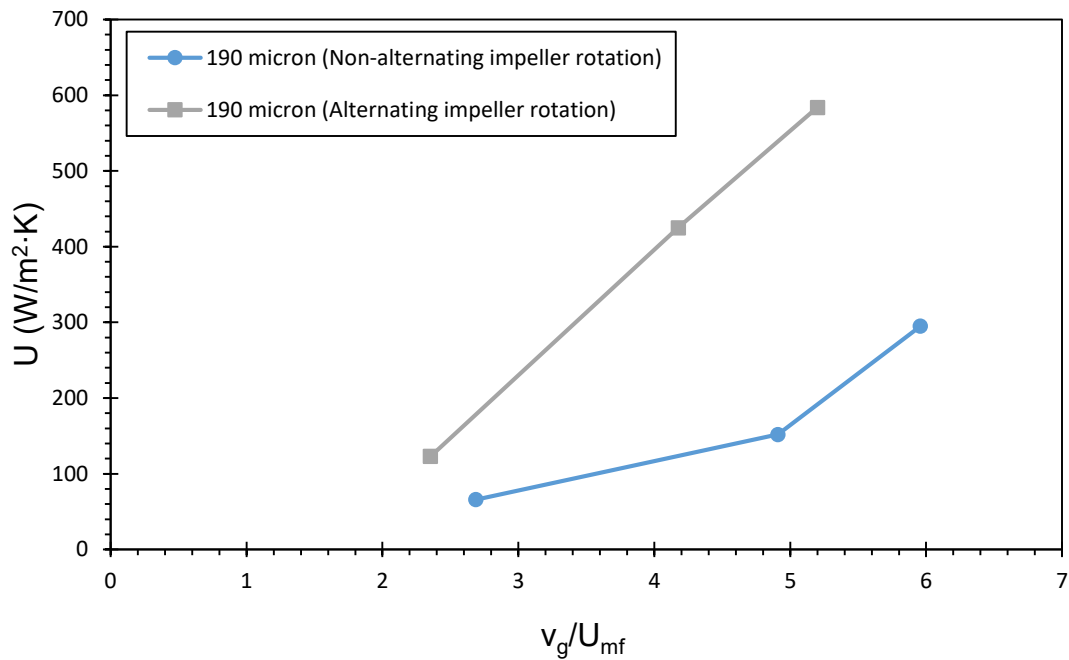
Figure 4-9: Overall heat transfer coefficient as a function of velocity ratio and the alternating or non-alternating impeller rotation with silica sand ($d_{p_{sm}} = 190$ µm).

Chapter 5

5   Effect of reactor volume, particle size and material on heat transfer in a mechanically fluidized reactor

5.1   Introduction

Scale-up of a bench-scale reactor is a considerable and essential task. This is especially important for the MFR, as the ratio of the wall surface to bed volume decreases with increasing reactor diameter, making heat transfer more critical in larger units.

The objective of this work is to compare the overall heat transfer coefficients measured in two reactors with different diameters: Small MFR and Large MFR. Efforts will then be made to correlate the observed heat transfer coefficients with the correlation given by Molerus et al. (1995). The effect of the impeller rotation speed on the heat transfer coefficient will also be studied for different particle sizes. Furthermore, experiments will use different particle materials (activated carbon and silica sand) to study the impact of the material properties. This study focuses on the effect of reactor scale on the wall-to-bed heat transfer coefficient in compact mechanically fluidized beds.

5.2   Materials

Particles used for the experiments performed in this Chapter are described in Section 2.3.

5.3   Methods

The experimental procedure followed has been previously discussed in Section 2.4.2.1. The wall-to-bed heat transfer coefficient measurement method has been described in Section 2.4.2.2. The studies presented in thus work were performed using two particle sizes in the Small Mechanically Fluidized Reactor (MFR).

IHM-2 is used for the experiments performed in this Chapter (refer to Appendix B for detailed specifications) as it has a very flexible heating process control and continuous supply of heat to the system can be provided. Some specifications of the induction system are given in Table 5-1.

In this chapter, superficial steam velocities reported are calculated at the freeboard conditions just above the bed temperature.

Table 5-1: Specification of the IHM-2.

Model	SI – 12KW
Voltage	230 V (3 phase)
Input Power	15 kVA
Output Power	12 kW

Detailed descriptions of the two MFRs can be found in Chapter 2. The sizing details of the studied reactors are provided in Table 5-2. The method used to measure the heat transfer coefficient from the MFR wall to the bed is described in section 2.4.2.2 (Chapter 2).

Table 5-2: MFR reactors vessel sizing details.

Dimensions	Units	Small MFR	Large MFR
Inner diameter	m	0.1015	0.15
Height	m	0.127	0.25
Total internal volume	L	1.03	4.42
Heat transfer area (Wall)	m^2	0.0405	0.1178

Equations required to estimate the overall heat transfer coefficient have been previously provided in Section 2.4.2.2. Heat transfer coefficients obtained for each experimental conditions are then compared with correlated values for standard fluidized beds, based on the correlation (8) by Molerus et al. (1995), which is stuitable for the type of particles used in this study, based on the Archimedes number (7).

5.4　　Results and Discussion

5.4.1　Small MFR with non-alternating rotation for the impeller

5.4.1.1　Wall-to-bed heat transfer for Sauter mean diameter of 600 μm

Several experiments were performed using the sand particles (Group B) with properties provided in Table 5-3.

Table 5-3: Properties of the sand particles ($d_{p_{sm}}$ = 600 μm).

Particle material	Particle Sauter mean diameter ($d_{p_{sm}}$)	Particle density (kg/m³)	Heat Capacity (J/kg/K)
Silica Sand	600 μm	2650	830

Runs were performed with different flow rates of liquid injection while varying the impeller rotation speeds. Following the injection of several liquid pulses using a syringe pump-syringe assembly (refer to **Figure 2-2**), the system is allowed to reach steady state. The power supplied (3 kW) from the IHM-2 (detailed in Appendix B) is continuous and results in elevated temperatures in the reactor wall. The wall temperature was measured at three different locations and reaches temperatures of approximately 600°C and the system is allowed to reach steady state before liquid injection is initiated.

Figure 5-1 presents the effect of the mixing speed and the superficial steam velocity on the bed temperature. The bed temperature was reduced as the superficial steam velocity increased from 42 mm/s to 110 mm/s. Increasing the liquid injection rate means that more heat must be transferred from the wall to cool the bed; if the bed wall is maintained at an approximately constant temperature, this means that the bed temperature must decrease to increase the heat transfer rate. The previous trend was expected as the increased heat requirements to evaporate the higher liquid injection resulted in a reduction of the bed temperature.

The relationship between bed temperature and mixer rotation speed varied depending on the superficial steam velocity. A relatively small increase in the bed temperature was observed when increasing the rotation speed for a superficial steam velocity of 42 mm/s and 80 mm/s. Conversely, the bed temperature was reduced when increasing the rotation speed for the highest studied superficial steam velocity of 110 mm/s which is an exception to the trend. The observed trends demonstrate the impact of rotation speed and liquid injection on the bed temperature. For a relatively low liquid injection, the rotation speed enhances the wall-to-bed heat transfer, thus increasing the bed temperature.
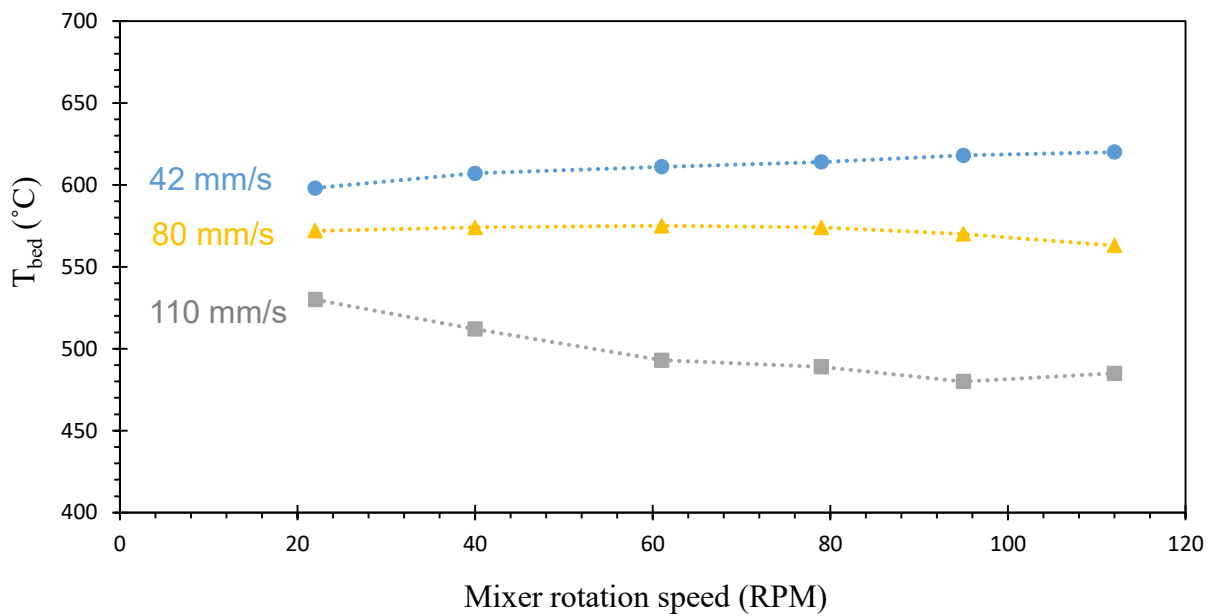
Figure 5-1: Effect of mixing speed on the measured bed temperature for superficial steam velocities. Silica sand $d_{p_{sm}}$ = 600 µm.

Figure 5-2 shows that the highest studied superficial steam velocity corresponded to the highest heat transfer coefficient between the reactor wall and bed, indicating better bed aeration and improved heat transfer. The estimated heat transfer coefficients generally increased with quicker rotation speeds, especially at higher superficial steam velocities. An exception was observed at high impeller speeds and the highest studied superficial steam velocity (110 mm/s), where the overall heat transfer coefficient was slightly reduced beyond 95 rpm. It is suspected that at high impeller rotation speeds, centrifugal forces result in a thin layer of nearly stationary bed material along the wall of the reactor, impairing heat transfer.

58

The particle Archimedes number (7) calculated at the different superficial velocities of steam are reported in Table 5-4.

The minimum fluidization velocity obtained using correlation provided by Richardson and S. Jeronimo (1979) is shown in Table 5-4, for the bed temperature corresponding to the three injection flowrates; it shows that the superficial gas velocity is much smaller than the minimum fluidization velocity and the bed is not fluidized properly. Hence, the overall heat transfer coefficient from correlation (Molerus et al., 1995) cannot be obtained for this particle size.

Table 5-4: Archimedes number calculated at corresponding steam velocities for particles $d_{p_{sm}} = 600$ μm.

Superficial steam velocity (mm/s)	Minimum fluidization velocity (mm/s)	Archimedes number
42	217	$1.46 * 10^3$
80	223	$1.63 * 10^3$
110	246	$2.19 * 10^3$

Experimental results show that the overall heat transfer coefficient increases with particle Archimedes number. And as the $10^2 < \text{Ar} < 10^5$, the gas convective heat transfer coefficient becomes dependent on the particles size as mentioned in Molerus (1995).
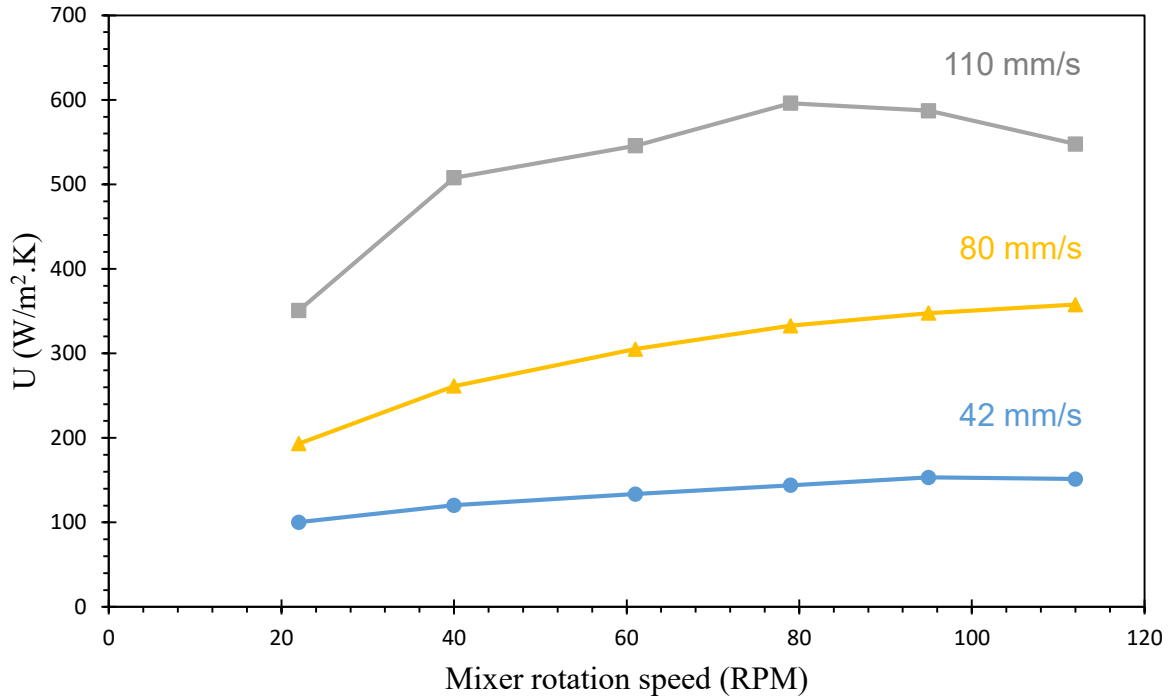
Figure 5-2: Overall heat transfer coefficient as a function of mixer rotation speed and superficial steam velocities. Silica sand $d_{p_{sm}}$ = 600 μm.

5.4.2   Large MFR with non-alternating rotation for the impeller

5.4.2.1   Wall-to-bed heat transfer using sand ($d_{p_{sm}}$ = 190 μm)

Several experiments were performed using the sand particles (Group B) with properties mentioned in Table 5-5 while studying the impact of liquid injection flow rates and impeller rotation speed. Following the injection on several liquid pulses using a syringe pump-syringe assembly (refer to Figure 2-2), the system reaches steady state.

Table 5-5: Properties of the smaller particles ($d_{p_{sm}}$ = 190 μm).

Particle material	Particle Sauter mean diameter ($d_{p_{sm}}$)	Particle density (kg/m³)	Heat Capacity (J/kg/K)
Silica Sand	190 μm	2650	830

The particle Archimedes number calculated at the different superficial velocities of steam are reported in Table 5-6. The minimum fluidization velocity obtained using correlation provided by Richardson and S. Jeronimo (1979) is shown in Table 5-6. The gas velocity for the smaller sand particles was extremely high when compared to the minimum fluidization velocity.

Table 5-6: Archimedes number, Minimum fluidization velocities calculated at corresponding steam velocities for particles $d_{p_{sm}}$ = 190 μm.

Superficial steam velocity (mm/s)	Minimum fluidization velocity (mm/s)	Archimedes number
503	39	$2.93 * 10^2$
528	44	$4.22 * 10^2$

Figure 5-3 presents the effect of the mixing speed and the liquid flow rate on the bed temperature. Superficial steam velocities of 503, 528 mm/s correspond to liquid flow rates of 250 ml/min, 290 ml/min (assuming steam properties at 190 ˚C, 160 ˚C respectively). The temperature of the bed falls as with an increase in liquid injection flow rate. The previous trend was expected as the increased heat requirements to evaporate the higher liquid injection flow resulted in a reduction of the bed temperature.
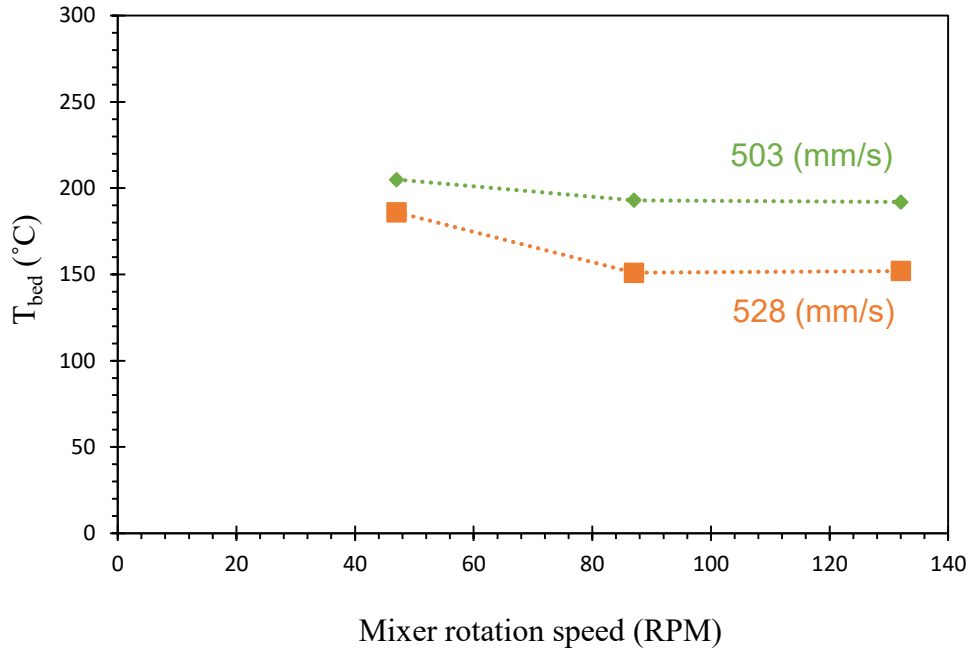
Figure 5-3: Effect of mixing speed on the bed temperature measurements with the change in superficial steam velocities. Silica sand $d_{p_{sm}}$ = 190 μm.

The overall heat transfer coefficient decreases sharply with the increase in the mixer speed for the two different superficial steam velocities (503 and 528 mm/s) as reported in Figure 5-4. The maximum value of heat transfer coefficient obtained at 47 rpm is surprising. Based on the trend followed by the small MFR (radius = 0.10 m or $5 * 10^{-2}$ cm) and using the sand with $d_{p_{sm}}$ = 190 μm the peak was obtained at 80 rpm (Chapter 4, Figure 4-5).

So in the case of large MFR (radius = 0.075 m or $7.75 * 10^{-2}$ cm) by assuming that the peak corresponds to the same centrifugal acceleration is at 80 rpm, we can calculate the optimum rpm. Thus, $80 * (5/7.5)^{0.5}$ = 65 rpm. This value of rpm gives us a scope to try many different rpm's so as to have a better understanding about the heat transfer in large MFR for the given particle size.
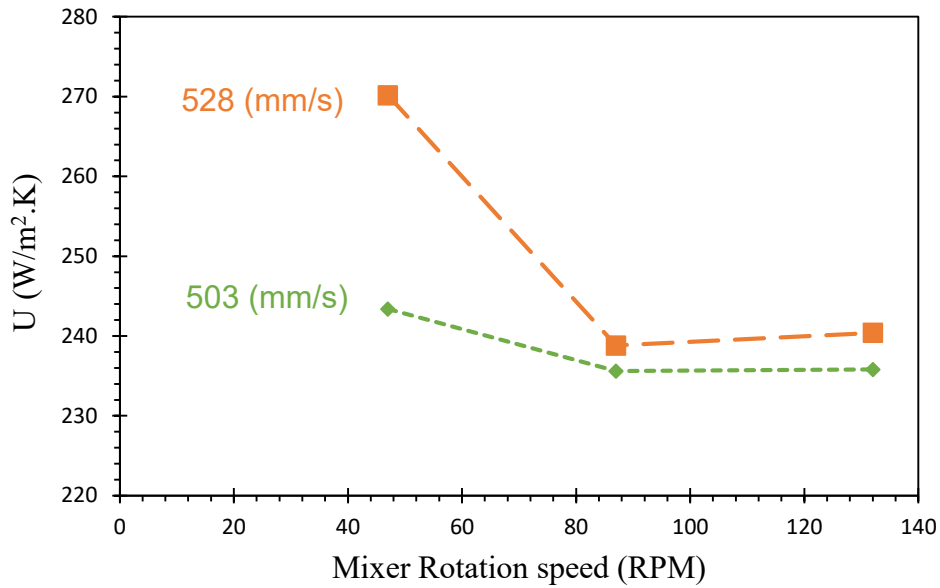
Figure 5-4: Overall heat transfer coefficient for different impeller rotation speeds and superficial steam velocities. Silica sand $d_{p_{sm}}$ = 190 μm.

Table 5-7 provides the overall heat transfer coefficients obtained with the large MFR. The overall heat transfer coefficient increased with at the higher superficial steam velocity. A more interesting analysis of the experimental results is obtained by comparing with the Molerus correlation. It is observed that the Molerus correlation for conventional fluidized beds provides comparable predictions for the studied 190 μm silica sand.

Table 5-7: Comparison between experimental overall heat transfer coefficient and Molerus correlation for $d_{p_{sm}}$ = 190 μm.

Flow rate (ml/min)	Superficial steam velocity (mm/s)	$U_{average}$ for studied RPM (W/m²·K)	U from correlation (W/m²·K)	U_{max} (W/m²·K)	$U_{max}/U_{correlation}$ (-)
250	503	238	280	243	0.87
290	528	250	261	270	1.03

5.4.2.2   Wall-to-bed heat transfer using activated carbon ($d_{p_{sm}}$ = 575 μm)

Experiments were performed using the activated carbon (Group B) with properties mentioned in Table 5-8 while studying the impact of the liquid injection flow rate and impeller rotation speeds. After injecting several liquid pulses using a syringe pump-syringe assembly (refer to Figure 2-2), the system reaches steady state.

Table 5-8: Properties of the activated carbon ($d_{p_{sm}}$ = 575 μm).

Particle material	Particle Sauter mean diameter (d$_{p_{sm}}$)	Particle density (kg/m³)	Heat Capacity (J/kg/K)
Activated Carbon	575 μm	750	1300

The particle Archimedes number calculated at the different superficial velocities of steam are reported in Table 5-9. The minimum fluidization velocity obtained using correlation provided by Richardson and S. Jeronimo (1979) is shown in Table 5-9. The gas velocity for the char particle was very high when compared to the minimum fluidization velocity.

Table 5-9: Archimedes number, Minimum fluidization velocities calculated at corresponding steam velocities for particles $d_{p_{sm}}$ = 575 μm.

Superficial steam velocity (mm/s)	Minimum fluidization velocity (mm/s)	Archimedes number
168	84	$4.68 * 10^3$
398	93	$6.36 * 10^3$

Figure 5-5 presents the effect of the mixing speed and liquid flow rate on the bed temperature. The liquid flow rates of 70 ml/min, 180 ml/min correspond to estimated superficial steam velocities of 168, 398 mm/s (assuming steam properties at 280 ℃, 235 ℃ respectively). The temperature of the bed shows a fall in the bed temperature on increasing the superficial steam velocity.
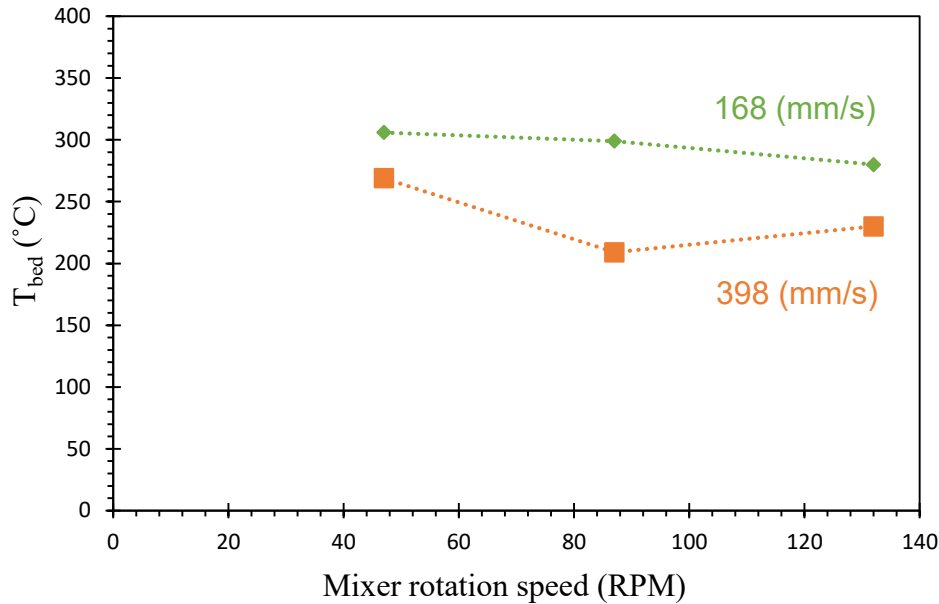
Figure 5-5: Effect of mixing speed on the bed temperature measurements with the change in liquid flow rate. Activated Carbon bed $d_{p_{sm}}$ = 575 μm.

Figure 5-6 presents the overall heat transfer coefficient, measured at various impeller rotation speeds and superficial steam velocities. As the superficial steam velocity increased, a significant effect on the overall heat transfer coefficient was observed. The increase in the impeller rotation speed have a small impact on the overall heat transfer coefficient for the bed of char. At high superficial steam velocity, the gas bubbles disrupt the formation of the layer of particles which makes them fall back into the reactor. This leads to a high overall heat transfer coefficient values even when operating at different impeller rotation speeds.
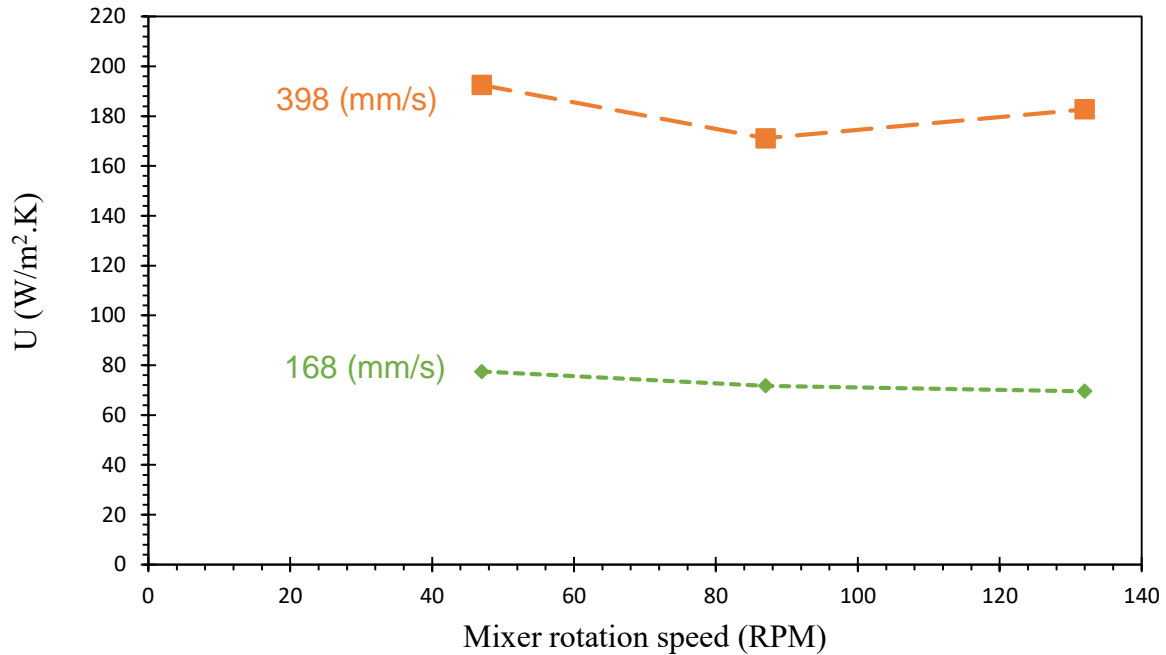
Figure 5-6: Overall heat transfer coefficient for different mixing speeds and superficial steam velocities. Activated Carbon bed $d_{p_{sm}}$ = 575 μm.

Table 5-10 shows that, the Molerus correlation gives an adequate approximation of the experimental results. This correlation can provide a rough estimate of the overall heat transfer coefficient.

Table 5-10: Comparison of the average overall heat transfer coefficient with the values from Molerus correlation for activated carbon $d_{p_{sm}}$ = 575 μm.

Flow rate (ml/min)	Superficial steam velocity (mm/s)	$U_{average}$ for studied RPM (W/m²·K)	U from correlation (W/m²·K)	U_{max} (W/m²·K)	$U_{max}/U_{correlation}$ (-)
70	168	73	104	77	0.74
180	398	182	124	192	1.55

Chapter 6

6 Conclusions and Recommendations

6.1 Conclusions

In this work, the experimental method of Reyes (2015) was successfully used to study the effect of impeller rotation speed and bed temperature on the properties of agglomerates formed in the Small MFR. Increasing the impeller rotation speed reduced the formation of larger agglomerates as the agglomerates break more easily and resulted in formation of smaller agglomerates. Also, increasing the bed temperature set-point reduced the amount of liquid trapped in macro-agglomerates.

A separate study on the effect of liquid flow rate and impeller rotation speed on the wall-to-bed overall heat transfer coefficient was performed in a Small MFR using silica sand. Experimental results demonstrated that higher superficial steam velocities corresponded to increased heat transfer coefficients between the wall and bed for both studied particle Sauter mean diameters (190 µm and 300 µm). This shows that the gas convective heat transfer becomes dependent on the size of the particle used for study based on Molerus (1993) correlation when $Ar > 10^8$. Experimental results were compared with the overall heat transfer coefficient obtained using Molerus et al. (1995) coefficient which shows that the overall heat transfer coefficient increases with the particle Archimedes number.

The effect of alternating rotation for the impeller was also completed in the Small MFR using silica sand with $d_{p_{sm}} = 190$ µm. The overall heat transfer coefficient almost doubled for the studied superficial steam velocities when using the alternating impeller rotation as the alternating rotation disrupts the relatively stable solid layer that forms at the wall and promotes surface renewal of the particles near the hot wall, enhancing heat transfer between the wall and the bed.

The overall heat transfer coefficient increased significantly with increasing particle size, as the heat transfer coefficient increases with increasing particle Archimedes number (Baskakov et al., 1973) which was the highest in comparison to the two smaller particle sizes (silica sand = 190, 300 µm) tested and at higher superficial steam velocities.

Silica sand with $d_{p_{sm}}$ = 600 µm resulted in the highest overall heat transfer coefficient at the maximum superficial steam velocity (110 mm/s).

In the case of activated carbon ($d_{p_{sm}}$ = 575 µm), the change in the overall heat transfer coefficient was not significant with the change in the impeller rotation speed.

6.2   Recommendations

It was observed when using Gum Arabic that increasing the bed temperature set-point beyond 130°C led to caramelization. It is recommended to investigate the use of different binder solutions to allow bed temperature set-points higher than 130℃, and to inject more liquid in a single pulse or multiple pulses. Furthermore, different dye colors can be used to evaluate the liquid spreading as the agglomerates are formed in the bed. The use of different dyes can help understand the pattern in which the agglomerates travel in the bed.

After the injection of second pulse is over, the mixing is stopped after 5 min in the current study but instead it is recommended to freeze the bed instantly or mixing at very low impeller rotation speed (5 rpm) for just 15 sec allowing the bed to stabilize and then freezing the bed. In this manner, different time intervals (30 secs, 60 secs) for which the mixing is allowed after the end of second pulse can be tried. Thus, the data obtained about the agglomerate formation can be extrapolated and it can lead to a better understanding with respect to the effect of mixing speed.

More values of the impeller rotation speed would need to be studied to understand the properties of agglomerates formed for the large MFR. Also, additional blades can be added to the impeller used in large MFR to study its effect on the heat transfer coefficient. It is also recommended to do more studies in large MFR with different particle sizes of silica sand and then comparison can be done based for the heat transfer coefficients measured in this work. Studying the impact of impeller geometry on the overall heat transfer coefficient in small MFR is also recommended. Finally, since the impeller alternating motion greatly improves the wall to bed heat transfer, its impact on liquid distribution should be determined.

The heat transfer study performed in small MFR using different liquid injection flow rates showed that the maximum liquid flow rate, and thus highest superficial steam velocity, corresponded to the highest overall heat transfer coefficient. Future work should perform more studies to investigate the operability limit for different reactor temperatures.

More studies can be performed to observe the effect of alternating impeller rotation on the overall heat transfer coefficient while changing the particle size and trying different bed materials (glass beads) for reactors with different diameter.

Appendices

Appendix A- Agglomerate formation study

A- 1 Silica sand and solvent solution mixture

The sample mixture prepared in order to have an estimate of the temperature set-point of the bed with which the experiments are to be performed is tested in an oven. The components of the mixture are:

Silica sand weighing 50 g (measured with the help of a scale with an accuracy of 0.1 mg) is taken in a beaker. The binder solution is separately prepared in a small beaker. It composition is: Gum Arabic solution weighing 5 gm (5 wt. % Gum Arabic, 2 wt. % dye, 93 wt. % water). The viscosity of the binder solution is adjusted using Hydrochloric acid (pH = 1.5). The binder solution is then mixed properly with the silica sand and the mixture is then spread on an aluminum foil as shown in figure A-2. This sample mixture is then placed in an oven. The temperature in the oven is set to 130 ˚C. The sample is kept in the oven for about 3h. The mixture is then carefully removed from the oven. The absorbance of this sample is obtained (the mixture sample is dissolved in water in a water to mixture ratio of 5:1) using an UV-vis Spectrophotometer.
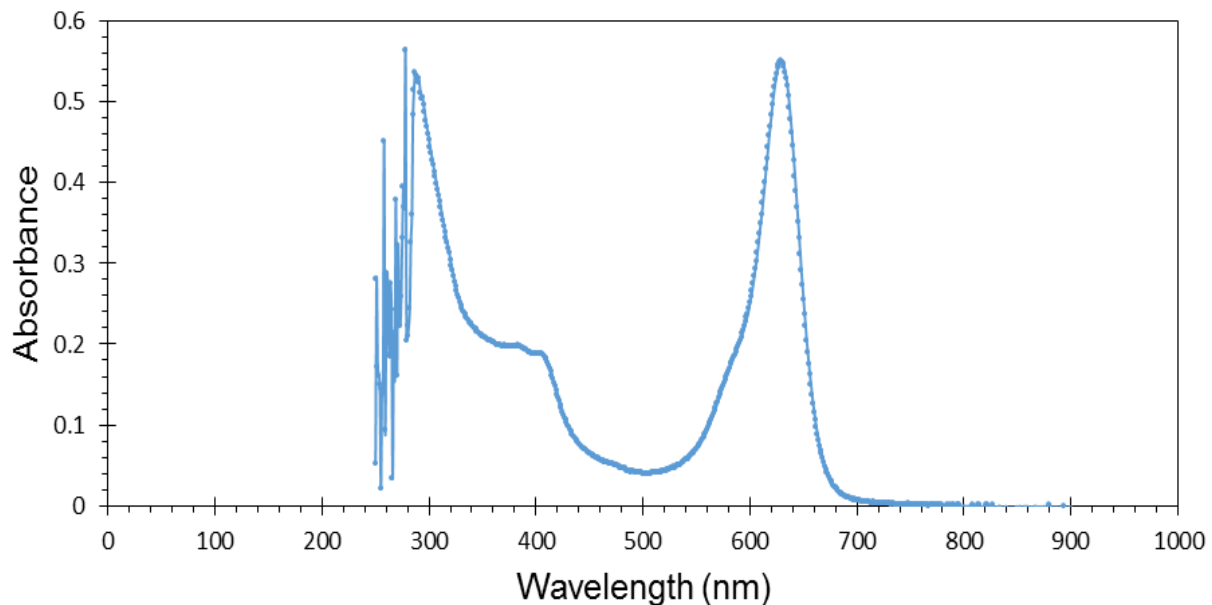
Figure A-1.1: With all 3 components of Gum Arabic solution (T_{SP} = 130 ˚C).
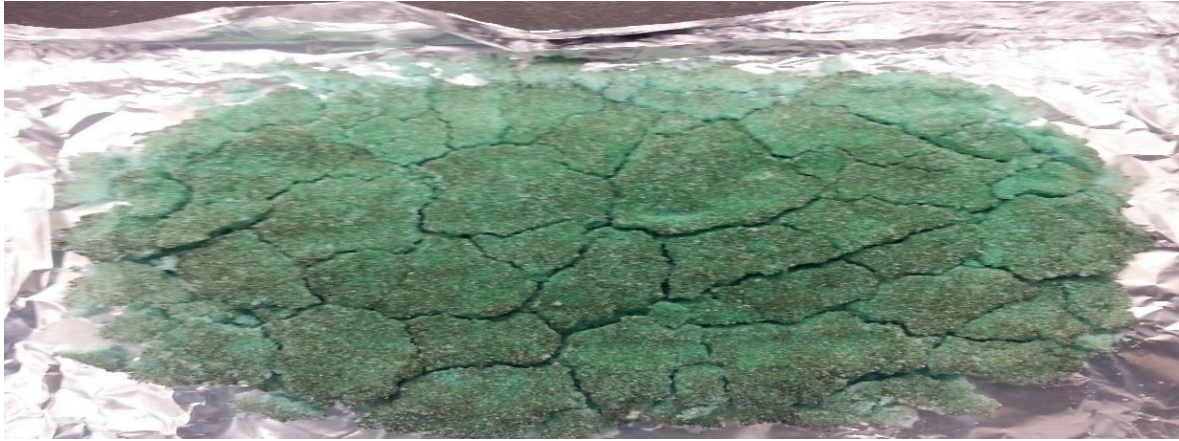
Figure A-1.2: The thermal degradation of Gum Arabic observed in a sample kept for observation in an oven.

A- 2 Sample calculation for % of liquid trapped

The amount of liquid trapped calculated using the values for the Avg. (L/S) which can then be compared to the amount of liquid trapped from the graphs plotted in the Results and Discussion section of Chapter 3.

Example:

(a) T_{SP} = 120 ˚C, Impeller rotation speed = 130 RPM

Total M_{sand} in agglomerates = 6.18 (g)

Avg. (L/S) = 0.16

Avg. (L) = 6.18*0.16 = 0.98 (g)

% liquid trapped = 0.98/40 = 2.5%

(a) T_{SP} = 130 ˚C, Impeller rotation speed = 130 RPM

Total M_{sand} in agglomerates = 2.03 (g)

Avg. (L/S) = 0.18

Avg. (L) = 2.03*0.18 = 0.36 (g)

% liquid trapped = 0.36/40 = 0.92%

A- 3 Small MFR Induction Heating System

The Small Mechanically Fluidized Reactor (MFR) is designed and equipped with custom built Induction Heating Machine (IMS-1). The heating machine comprise of 1800 W induction heater (Hannex, Hong Kong, China) which is used to regulate the reactor temperature.

The system is suitable for use on a circuit capable of delivering not more than 5000 RMS Symmetrical Amperes and 120 V Maximum. The system has got more than one power supply (120*2 V, 1A/15A, 60 HZ and single phase system) and is an accepted form of approval of electrical products by the Electrical Safety Authority.

Temperature readings for the reactor were acquired at different locations along the wall of the reactor, vapor temperature in the freeboard region and in the bed of the reactor using five type K thermocouples, two 4-channel thermocouple input (NI-9211 from National Instruments, Austin, TX), and one Bus-Powered Multifunctional DAQ USB Drive (NI USB-6009 from National Instruments, Austin, TX). Program created using the LabWindows ™/CVI platform (National Instruments, Austin, TX) helped collecting the temperature signals and an ON-OFF controller is used to power the induction heating system.

Induction heating system is capable of reaching temperatures of about 450-500°C in 30-40 minutes for the small MFR.

Table A- 3.1: Specifications of the induction heating system using IHM-1.

Induction Power Supply	Wattage	1800 W
	Frequency	33 kHz
Induction wiring	Wiring specifications	Vibraflame® extreme temperatures composite wire- 14 AWG
	Total wire length	13 m
	Small MFR wiring	26 loops

A-4 (a) Sample calculation for L/S ratio

The experiment is performed at T_{SP} = 120 ˚C, Impeller rotation speed = 40 rpm, F_L = 4 ml/min.

Table A- 4.1: Example of the calculation for agglomerates study in Chapter 3.

Part -1:

Size cut (μm)	Absorbance	Concentration of dye (wt. %)	Weight of all cuts (g)	Water	Pure blue	Blue Solution [actual] (g)	Gum Arabic (g)
9500	0.68	6.1E-06	3.1	15.5	9.5 E-05	0.0098	0.0245
4000	0.92	8.3E-06	1.3	6.5	5.4 E-05	0.0056	0.0139
2000	0.35	3.2 E-06	0.32	1.6	5.1 E-06	0.0005	0.0013
1400	0.74	6.7 E-06	0.21	1.05	7.0 E-06	0.0007	0.0018
850	0.9	8.1 E-06	0.24	1.2	9.7 E-06	0.001	0.0025
600	0.74	6.6 E-06	0.28	1.4	9.3 E-06	0.001	0.0024
500	0.57	5.1 E-06	0.28	1.4	7.1 E-06	0.0007	0.0018
425	0.34	3.0 E-06	0.9	4.5	1.4 E-05	0.0014	0.0035
355	0.21	1.9 E-06	3.45	17.25	3.3 E-05	0.0034	0.0084

Part-2:

Size cut (µm)	Water trapped (g)	Water trapped (%)	Cumulative % of water trapped	Whole solution (g)	M_{sand} in agglomerates (g)	L/S
9500	0.46	1.22	1.22	0.49	3.08	0.16
4000	0.26	0.69	1.92	0.28	1.29	0.22
2000	0.02	0.07	1.98	0.03	0.32	0.08
1400	0.03	0.09	2.07	0.04	0.21	0.17
850	0.05	0.13	2.2	0.05	0.24	0.21
600	0.04	0.12	2.32	0.05	0.28	0.17
500	0.03	0.09	2.41	0.04	0.35	0.11
425	0.07	0.18	2.59	0.07	0.58	0.12
355	0.16	0.42	3.01	0.17	0.47	0.36

Part-3:

For micro-agglomerates	Blue + Gum Arabic (g)	M_{sand} (g)	X_f for 215 µm (%)	X_{fbed} for 215 µm (%)	m_p (g)	$M\mu_{aggl}$ (g)
500	0.0018	0.3	60.20	47.78	0.35	0.35
425	0.0035	0.9	30.95	47.78	0.58	0.58
355	0.0085	3.4	6.56	47.78	0.47	0.48

A-4 (b) Different number of runs at each operating conditions

Table A- 4.2 provides the data for the weight percentage of liquid trapped for each run and their average while operating at different impeller rotation speeds.

Table A- 4.2: Details of the wt. % of liquid trapped at different operating conditions for each run. T$_{SP}$ = 120 ˚C.

	Wt. % of liquid trapped at T_{SP} = 120 ˚C				
Size cuts (μm)	Run 1	Run 1	Run 1	Run 2	Average
	(40 RPM)	(95 RPM)	(130 RPM)	(130 RPM)	(130 RPM)
4000	0.73	0.60	0.10	0.16	0.13
2000	0.07	0.04	0.49	0.36	0.42
1400	0.10	0.07	0.14	0.06	0.10
850	0.13	0.13	0.18	0.07	0.12
600	0.13	0.22	0.43	0.42	0.42
500	0.10	0.21	0.27	0.28	0.27
425	0.19	0.34	0.37	1.02	0.70
355	0.44	0.83	0.89	0.59	0.74

Tables A- 4.3, A- 4.4 and A- 4.5 provide the data for the weight percentage of liquid trapped for each run and their average while operating at different impeller rotation speeds.

Table A- 4.3: Details of the wt.% of liquid trapped for each run at impeller rotation speed = 40 rpm. T$_{SP}$ = 130 ˚C.

Wt. % of liquid trapped at T_{SP} = 130 ˚C				
Size cuts (μm)	Run 1	Run 2	Run 3	Average
4000	0.09	1.23	0.74	0.69
2000	0.08	0.96	0.45	0.50
1400	0.02	0.20	0.26	0.16
850	0.10	0.52	0.48	0.37
600	0.22	0.46	0.49	0.39
500	0.21	0.33	0.25	0.26
425	0.35	0.61	0.90	0.62
355	0.64	0.96	0.48	0.69

Table A- 4.4: Details of the wt.% of liquid trapped for each run at impeller rotation speed = 95 rpm. T$_{SP}$ = 130 ˚C.

Wt. % of liquid trapped at T_{SP} = 130 ˚C				
Size cuts (µm)	Run 1	Run 2	Run 3	Average
4000	0.22	0.05	0.09	0.12
2000	0.01	0.06	0.11	0.06
1400	0.01	0.05	0.09	0.05
850	0.04	0.01	0.07	0.04
600	0.09	0.02	0.02	0.04
500	0.07	0.01	0.08	0.05
425	0.11	0.10	0.16	0.12
355	0.44	0.33	0.47	0.42

Table A- 4.5: Details of the wt.% of liquid trapped for each run at impeller rotation speed = 130 rpm. T$_{SP}$ = 130 ˚C.

Wt. % of liquid trapped at T_{SP} = 130 ˚C			
Size cuts (µm)	Run 1	Run 2	Average
4000	0.23	0.05	0.14
2000	0.07	0.04	0.05
1400	0.03	0.01	0.02
850	0.12	0.06	0.09
600	0.14	0.06	0.10
500	0.08	0.22	0.15
425	0.15	0.13	0.14
355	0.50	0.31	0.41

Table A- 4.6 provides the data for the weight percentage of agglomerates in the bed for each run and their average while operating at different impeller rotation speeds.

Table A- 4.6: Details of the wt. % of agglomerates in the bed at different operating conditions for each run. T$_{SP}$ = 120 ˚C.

Wt. % of agglomerates in the bed at T_{SP} = 120 ˚C				
Size cuts (µm)	Run 1 (40 RPM)	Run 1 (95 RPM)	Run 1 (130 RPM)	Run 2 (130 RPM)	Average (130 RPM)
4000	0.33	0.29	0.05	0.09	0.07
2000	0.08	0.02	0.21	0.19	0.20
1400	0.05	0.03	0.07	0.03	0.05
850	0.06	0.09	0.13	0.08	0.10
600	0.07	0.14	0.20	0.22	0.21
500	0.07	0.17	0.12	0.17	0.14
425	0.23	0.32	0.26	0.53	0.39
355	0.86	1.11	1.20	1.28	1.24

Tables A- 4.7, A- 4.8 and A- 4.9 provide the data for the weight percentage of agglomerates in the bed for each run and their average while operating at different impeller rotation speeds.

Table A- 4.7: Details of the wt. % of agglomerates in the bed at impeller rotation speed = 40 rpm. T$_{SP}$ = 130 ˚C.

Wt. % of agglomerates in the bed at T_{SP} = 130 ˚C				
Size cuts (µm)	Run 1	Run 2	Run 3	Average
4000	0.19	0.58	0.49	0.42
2000	0.07	0.45	0.28	0.27
1400	0.02	0.13	0.21	0.12
850	0.07	0.34	0.37	0.26
600	0.16	0.31	0.39	0.29
500	0.14	0.21	0.22	0.19
425	0.32	0.33	0.42	0.35
355	1.12	1.2	1.23	1.18

Table A- 4.8: Details of the wt. % of agglomerates in the bed at impeller rotation speed = 95 rpm. T$_{SP}$ = 130 ˚C.

Wt. % of agglomerates in the bed at T_{SP} = 130 ˚C				
Size cuts (µm)	Run 1	Run 2	Run 3	Average
4000	0.28	0.13	0.09	0.16
2000	0.03	0.09	0.10	0.07
1400	0.01	0.07	0.06	0.05
850	0.02	0.03	0.06	0.04
600	0.06	0.03	0.01	0.03
500	0.07	0.05	0.08	0.06
425	0.17	0.17	0.24	0.19
355	1.00	0.99	1.10	1.03

Table A- 4.9: Details of the wt. % of agglomerates in the bed at impeller rotation speed = 130 rpm. T$_{SP}$ = 130 ˚C.

Wt. % of agglomerates in the bed at T_{SP} = 130 ˚C			
Size cuts (µm)	Run 1	Run 2	Average
4000	0.16	0.08	0.12
2000	0.04	0.02	0.03
1400	0.02	0.01	0.01
850	0.06	0.04	0.05
600	0.06	0.03	0.04
500	0.05	0.10	0.07
425	0.23	0.42	0.32
355	1.12	1.16	1.14

Appendix B- Heat Transfer study

B- 1 Induction Heating System used for Small MFR and Large MFR

The Small Mechanically Fluidized Reactor (MFR) is using a different induction heating system to carry out all the experiments related to Chapter 4, 5. The Induction Heating Machine (IMS-2) has a very flexible heating process control. IMS-2 is a medium frequency (30-80 kHz) induction heater (Superior Induction Company, Pasadena, CA).

The use of the previous Induction Heating Machine discussed in Appendix A- Agglomerate formation study is not done as higher temperature conditions and continuous supply of heat to the system are the requirements for all the tests. A much more powerful system with high heating speed, therefore, needs to be used. All the tests done with Small MFR and Large MFR uses IHM-2. Below mentioned are some of its specifications:

Table B- 1.1: Specifications of the induction heating system using IHM-2.

Model	SI – 12KW
Voltage	230 V (3 phase)
Input Power	15 kVA
Output Power	12 kW
Output Frequency	30 – 80 kHz
Output Current	1000 A
Auto Heating Time	1 – 99 seconds
Auto Cooling Time	1 – 99 seconds
Air Cooling	Rear Fan
Heat- Station Weight	~ 35 kg

The induction system uses copper coil which are wrapped carefully on the walls of the reactor and then connected to the terminals on the induction unit. The system uses water at a certain flow rate for cooling itself and allows the continuous flow of water from the two inlet ports at the back of the Heat- Station. Also, there are four outlet ports situated at the back of the Heat- Station (for the heated water which comes from the coil wrapped on the walls of the reactor) which are then connected using four tubes to a single water exit pipe and the water can thus be drained.

Figure B- 1.1: The Heat-Station of the induction heating system using IHM-2.

For experiments performed with Small MFR, about 3 kW of power is supplied for heating requirements. Similarly, the experiments performed with Large MFR uses the IHM-2. The power supplied in order to carry out the experiments in the Large MFR is about 6.5 kW. This allows the system to be rapidly heated and achieve a very high temperature in the bed and the wall of the reactor given its bigger size compared to the Small MFR.

B-2 Sample Overall Heat Transfer Coefficient Calculation

The experiment is performed at F_L = 5 ml/min (8.33E-05 kg/s) and different impeller rotation speeds.

Table B- 2.1: Example of the calculation for Overall Heat Transfer Coefficient for Chapter 4, 5.

RPM	T_{bed} (˚C)	T_1 (˚C)	T_2 (˚C)	T_3 (˚C)	$T_{w_{average}}$ (˚C)	$T_{w_{STDEV}}$ (˚C)	ΔH_v $(\frac{kJ}{kg})$	U $\left(\frac{W}{m^2.K}\right)$
0	587	673	755	778	735.3	55.2	3583.5	49.7
22	615	677	740	788	735	55.6	3641.7	62.4
40	622	676	745	789	736.6	56.9	3656.3	65.6
61	624.5	680	744	783	735.6	52.0	3661.5	67.7
79	625.5	685	745	783	737.6	49.4	3663.6	67.2
95	625	692	744	783	739.6	45.6	3662.5	65.7
112	624	698	744	783	741.6	42.5	3660.4	64.0

Table B- 2.2: Input for calculating the superficial gas velocity.

GAS DENSITY	kg/m^3	0.24
GAS VISCOSITY	kg/s/m	3.36E-05
GAS THERMAL CONDUCTIVITY	W/ (m. K)	0.083
GAS HEAT CAPACITY	J/ (kg. K)	2220.5
LIQUID FLOWRATE	kg/s/m	8.33E-05
SUPERFICIAL GAS VELOCITY	m/s	0.0426
	mm/s	43

Reference

Ayazi Shamlou, A., Liu, Z., Yates, J.G., 1990. Hydrodynamic influences on particle breakage in fluidized beds. Chem. Eng. Sci. 45, 809–817. doi:10.1016/0009-2509(90)85004-W

Baskakov, A.P., Berg, B. V., Vitt, O.K., Filippovsky, N.F., Kirakosyan, V.A., Goldobin, J.M., Maskaev, V.K., 1973. Heat transfer to objects immersed in fluidized beds. Powder Technol. 8, 273–282. doi:10.1016/0032-5910(73)80092-0

Basu, P., Nag, P.K., 1987. An investigation into heat transfer in circulating fluidized beds. Int. J. Heat Mass Transf. 30, 2399–2409. doi:10.1016/0017-9310(87)90230-4

Benali, M., Gerbaud, V., Hemati, M., 2009. Effect of operating conditions and physico–chemical properties on the wet granulation kinetics in high shear mixer. Powder Technol. 190, 160–169. doi:10.1016/j.powtec.2008.04.082

Botterill, J.S.M., 1975. Fluid-bed heat transfer. Gas-fluidized bed behaviour and its influence on bed thermal properties. Academic Press,New York, United States.

Bridgwater, A.V., 2012. Review of fast pyrolysis of biomass and product upgrading. Biomass and Bioenergy 38, 68–94. doi:10.1016/j.biombioe.2011.01.048

Chaudhari, M., 2012. Effect of Liquid-Solid Contact on Thermal Cracking of Heavy Hydrocarbons in a Mechanically Fluidized Reactor.

Daizo, K., Levenspiel, O., 1991. Fluidization engineering, 2nd edition. Stoneham, MA (United States); Butterworth Publishers, United States.

Di Natale, F., Lancia, A., Nigro, R., 2009. Surface-to-bed heat transfer in fluidised beds of fine particles. Powder Technol. 195, 135–142. doi:10.1016/j.powtec.2009.05.024

Flury, M., Flühler, H., 1994. Brilliant Blue FCF as a Dye Tracer for Solute Transport Studies—A Toxicological Overview. J. Environ. Qual. 23, 1108. doi:10.2134/jeq1994.00472425002300050037x

Gel'perin, N.I., Ainshtein, V.G., 1971. A method of determining the interphase heat-transfer coefficient in a fluidized bed of granular materials 13, 69–70. doi:10.1007/BF00831757

Gray, M.R., 2002. Fundamentals of bitumen coking processes analogous to granulations: A critical review. Can. J. Chem. Eng. 80, 393–401. doi:10.1002/cjce.5450800308

Hammond, D.G., Lampert, L.F., Mart, C.J., Massenzio, S.F., Phillips, G.E., Sellards, D.L., Woerner, A.C., 2003. Refining: Review of fluid bed coking technologies. Pet. Technol. Q. 8, 27–31, 33.

House, P., Berruti, F., Gray, M., Chan, E., Briens, C., 2006. Prediction of propensity to fouling in fluid cokers, in: AIChE National Meeting, San Francisco.

House, P.K., Briens, C.L., Berruti, F., Chan, E., 2008. Effect of spray nozzle design on liquid–solid contact in fluidized beds. Powder Technol. 186, 89–98. doi:10.1016/j.powtec.2007.11.005

House, P.K., Saberian, M., Briens, C.L., Berruti, F., Chan, E., 2004. Injection of a liquid spray into a fluidized bed: Particle-liquid mixing and impact on fluid coker yields. Ind. Eng. Chem. Res. 43, 5663–5669. doi:10.1021/ie034237q

Imeson, A., 2009. Food Stabilisers, Thickeners and Gelling Agents, Food Stabilisers, Thickeners and Gelling Agents. Wiley-Blackwell.

Iveson, S.M., Litster, J.D., Hapgood, K., Ennis, B.J., 2001. Nucleation, growth and breakage phenomena in agitated wet granulation processes: A review. Powder Technol. doi:10.1016/S0032-5910(01)00313-8

Iveson, S.M., Page, N.W., 2001. Tensile bond strength development between liquid-bound pellets during compression. Powder Technol. 117, 113–122. doi:10.1016/S0032-5910(01)00319-9

Kee Soo Han, Hyung Jin Sung, Myung Kyoon Chung, 1991. Analysis of heat transfer in a pipe carrying two-phase gas-particle suspension. Int. J. Heat Mass Transf. 34, 69–78.

doi:10.1016/0017-9310(91)90174-D

Lago, V., Greenhalf, C., Briens, C., Berruti, F., 2015. Mixing and operability characteristics of mechanically fluidized reactors for the pyrolysis of biomass. Powder Technol. 274, 205–212. doi:10.1016/j.powtec.2014.11.038

McKendry, P., 2002. Energy production from biomass (part 3): gasification technologies. Bioresour. Technol. 83, 55–63. doi:10.1016/S0960-8524(01)00120-1

McMillan, J., Shaffer, F., Gopalan, B., Chew, J.W., Hrenya, C., Hays, R., Karri, S.B.R., Cocco, R., 2013. Particle cluster dynamics during fluidization. Chem. Eng. Sci. 100, 39–51. doi:10.1016/j.ces.2013.02.047

Mehta, K.A., Rekhi, G.S., Parikh, D.M., 2005. Extrusion/Spheronization as a Granulation Technique, in: Handbook of Pharmaceutical Granulation Technology. pp. 333–363. doi:10.1201/9780849354953.ch17

Mickley, H.S., Fairbanks, D.F., 1955. Mechanism of heat transfer to fluidized beds. AIChE J. 1, 374–384. doi:10.1002/aic.690010317

Molerus, O., 1993. Arguments on heat transfer in gas fluidized beds. Chem. Eng. Sci. 48, 761–770. doi:10.1016/0009-2509(93)80142-D

Molerus, O., Burschka, a., Dietz, S., 1995. Particle migration at solid surfaces and heat transfer in bubbling fluidized beds -- II. Prediction of heat transfer in bubbling fluidized beds. Chem. Eng. Sci. 50, 879–885. doi:10.1016/0009-2509(94)00446-X

Parveen, F., Josset, S., Briens, C., Berruti, F., 2012. Effect of size and density on agglomerate breakage in a fluidized bed 231, 102–111. doi:10.1016/j.powtec.2012.07.055

Pont, V., Saleh, K., Steinmetz, D., Hémati, M., 2001. Influence of the physicochemical properties on the growth of solid particles by granulation in fluidized bed. Powder Technol. 120, 97–104. doi:10.1016/S0032-5910(01)00355-2

Reyes, L.P., 2015. Effect of Temperature and Successive Sprays on Liquid Distribution in Fluidized Beds. Electron. Thesis Diss. Repos.

Richardson, J.F., da S. Jerónimo, M.A., 1979. Velocity-voidage relations for sedimentation and fluidisation. Chem. Eng. Sci. 34, 1419–1422. doi:10.1016/0009-2509(79)85167-2

Saha, M., 2012. SIMULTANEOUS PARTICLE AGGLOMERATION AND ATTRITION IN A HIGH Mithun Saha Simultaneous particle agglomeration and attrition in a high temperature fluidized bed. doi:10.1163/156855200750172286

Sauke, T.B., Becker, J.F., 1998. Stable isotope laser spectrometer for exploration of Mars. Planet. Space Sci. 46, 805–812. doi:10.1016/S0032-0633(98)00014-2

Schæfer, T., Mathiesen, C., 1996. Melt pelletization in a high shear mixer. IX. Effects of binder particle size. Int. J. Pharm. 139, 139–148. doi:10.1016/0378-5173(96)04548-6

Soskind, D.M., Spektor, G.S., Kasatkin, D.F., Zenchenkova, M.G., 1982. Fluid coking of heavy resids. Chem. Technol. Fuels Oils 18, 483–488. doi:10.1007/BF00725441

Stanlick, C., 2014. The Effects of Mixing and Vapor Residence Time on the Thermal Cracking Performance of Fluidized Beds.

Stefanova, A., Bi, H.T., Lim, J.C., Grace, J.R., 2011. Local hydrodynamics and heat transfer in fluidized beds of different diameter. Powder Technol. 212, 57–63. doi:10.1016/j.powtec.2011.04.026

Syamlal, M., Gidaspow, D., 1985. Hydrodynamics of fluidization: Prediction of wall to bed heat transfer coefficients. AIChE J. 31, 127–135. doi:10.1002/aic.690310115

Weber, S., Briens, C., Berruti, F., Chan, E., Gray, M., 2011. Stability of agglomerates made from fluid coke at ambient temperature 209, 53–64. doi:10.1016/j.powtec.2011.02.004

Weber, S., Briens, C., Berruti, F., Chan, E., Gray, M., 2008. Effect of agglomerate properties on agglomerate stability in fluidized beds. Chem. Eng. Sci. 63, 4245–4256.

doi:10.1016/j.ces.2008.05.035

Woollard, I.N.M., Potter, O.E., 1968. Solids mixing in fluidized beds. AIChE J. 14, 388–391. doi:10.1002/aic.690140310

Yang, Y., Anvari, M., Pan, C.-H., Chung, D., 2012. Characterisation of interactions between fish gelatin and gum arabic in aqueous solutions. Food Chem. 135, 555–561. doi:10.1016/j.foodchem.2012.05.018

Yao, X., Zhang, Y., Lu, C., Han, X., 2015. Systematic study on heat transfer and surface hydrodynamics of a vertical heat tube in a fluidized bed of FCC particles. AIChE J. 61, 68–83. doi:10.1002/aic.14635

Curriculum Vitae

Name: Dhiraj Kankariya

Post-secondary   Vishwakarma Institute of Technology
Education and   Pune, Maharashtra, India
Degrees: 2010-2014 Bachelor of Technology (B. Tech) in Chemical Engineering

                    The University of Western Ontario
                    London, Ontario, Canada
                    2014-2016 MESc in Chemical and Biochemical Engineering

Honors and   Western Graduate Scholarship
Awards: 2014-2016

Related Work   Graduate Research Assistant
Experience   ICFAR, The University of Western Ontario
                    London, Ontario, Canada
                    2014-2016

                    Graduate Teaching Assistant
                    The University of Western Ontario
                    London, Ontario, Canada
                    2015-2016